

Study of transport coefficients in ultrarelativistic kinetic theory

Victor E. Ambruş^{1,*}

¹*Department of Physics, West University of Timișoara,
Bd. Vasile Pârvan 4, 300223 Timișoara, Romania*

(Dated: October 12, 2018)

Abstract

The connection between the relativistic Boltzmann equation and the dissipative hydrodynamics equations is traditionally made through the Chapman-Enskog procedure or through Grad's moment approximation. While the ensuing transport coefficients predicted by the two approaches coincide in the non-relativistic limit, in general their ultra-relativistic limits differ. In this paper, we consider a spatially-periodic longitudinal wave in relativistic dissipative hydrodynamics. At sufficiently small wave amplitudes, we obtain an analytic solution in the linearised limit of the macroscopic conservation equations within the first- and second-order relativistic hydrodynamics formulations. We then use a kinetic solver to obtain the numerical solution of the relativistic Boltzmann equation for massless particles in the Anderson-Witting approximation for the collision term. We find that the transport coefficients emerging from the relativistic Boltzmann equation agree with those predicted through the Chapman-Enskog procedure. We further strengthen this claim by considering a moment-type approximation based on orthogonal polynomials under which the Chapman-Enskog results for the transport coefficients are exactly recovered.

* E-mail: victor.ambrus@e-uvt.ro

I. INTRODUCTION

The relativistic Boltzmann equation is known to reduce to the equations of relativistic hydrodynamics in the limit when the mean free path of the particle constituents is negligible compared to the typical length scales of the system [1]. The transition from kinetic theory to relativistic hydrodynamics is traditionally performed following two approaches: the Chapman-Enskog procedure and Grad's 14 moments approximation [1]. These two approaches yield different expressions for the transport coefficients appearing in the constitutive equations of the underlying hydrodynamic equations. While the non-relativistic limit of these expressions coincides between the two formulations, their ultrarelativistic limits differ.

In order to check which one of the two approaches (Chapman-Enskog expansion or the Grad method) correctly predicts the transport coefficients of the hydrodynamic equations, a solution of the relativistic Boltzmann equation is required. Solving the Boltzmann equation requires an explicit expression for the collision term, which in general is an integral operator taking into account local binary collisions. A considerable simplification arises by employing a single relaxation time (SRT) approximation. The most common SRT approximations are the Marle [2] and the Anderson-Witting [3, 4] models, which generalise the widely-used Bhatnagar-Gross-Krook (BGK) model introduced in Ref. [5] for the non-relativistic case. Since it is known that the Marle model is not appropriate for the study of the flow of massless particles [1, 3], we will only consider the Anderson-Witting model in this paper.

There has been recent evidence in the literature indicating that the transport coefficients predicted by the Chapman-Enskog method are closer to those recovered from solutions of the Boltzmann equation than those obtained through Grad's 14 moment approximation.

Florkowski et al. obtained a solution of the Anderson-Witting-Boltzmann (AWB) equation in the case of Bjorken flow [6] at non-vanishing relaxation time, written in integral form for the case when the distribution function depends only on proper time. This solution was restricted to the massless case in Refs. [7, 8] and extended to the massive case in Ref. [9]. In Refs. [7, 8], it is shown that the numerical solution of the Israel-Stewart equations [10] leads to better agreement with the AWB solution (computed also numerically) when the Chapman-Enskog value for the shear viscosity η is used compared to when the 14 moment approximation is used. The same conclusion is reached in Ref. [11] for the case of

Bose-Einstein and Fermi-Dirac statistics.

The solution of the AWB equation describing the Bjorken flow of massive particles obtained in Ref. [9] is used in Ref. [12] to highlight that the second-order Chapman-Enskog expansion is in closest agreement to the solution of the AWB equation as compared to the Israel-Stewart and the 14 moment approaches introduced in Refs. [10] and [13], respectively.

In Ref. [14], Bhalerao et al demonstrated that a Chapman-Enskog-like approximation of the non-equilibrium distribution function yielded a closer agreement with the inviscid limit of the Bjorken flow than the Grad approximation.

The relativistic lattice Boltzmann (LB) method has also been used as a tool to solve the AWB equation [15–24]. The propagation of planar shock waves of massless [15, 17–20] and massive [22, 23] particles was investigated using the LB method and the results were validated by comparison with the data obtained using the Boltzmann Approach to Multi Parton Scattering (BAMPS) reported in Refs. [25–27]. In order to compare the LB results obtained in the frame of the AWB equation and the BAMPS results, the shear viscosity to entropy ratio η/s must be kept constant. Matching within the LB method the values of η/s employed in the BAMPS simulations requires as an input the exact expression for the shear viscosity η , which can be obtained via Grad’s 14 moment approach [15, 17–19, 22] or the Chapman-Enskog procedure [20, 23]. The authors of Refs. [20, 23] note that employing the Chapman-Enskog value for η leads to better agreement with the BAMPS data than when the Grad value is employed.

Recently, the relativistic lattice Boltzmann model developed in Ref. [22] was used in Ref. [23] to study the dissipative attenuation of the relativistic equivalent of the Taylor-Green vortices. This study allowed the authors of Ref. [23] to demonstrate that the correct value of the shear viscosity is that given by the Chapman-Enskog procedure rather than the Grad method for a wide range of particle masses.

In this paper, we present a study of the transport coefficients and second-order relaxation times arising in the Anderson-Witting model by considering the dissipative attenuation of a harmonic longitudinal wave. We focus on three regimes of wave propagation, corresponding to the cases when the velocity β along the wave propagation direction (*Case 1*), pressure $P = P_0 + \delta P$ (*Case 2a*) or density $n = n_0 + \delta n$ (*Case 2b*) are perturbed harmonically about $\beta = 0$, $n = n_0$ and $P = P_0$. In each case, the other two macroscopic variables are left unperturbed in the initial state. In all cases, we assume that at initial time, the fluid

is in local thermodynamic equilibrium characterised by the Maxwell-Jüttner distribution corresponding to the local values of n , P and β . The analytic analysis of this system is restricted to the regime of small amplitudes β_0 , δn_0 and δP_0 , where the linearised form of the macroscopic equations can be solved analytically.

In the first-order description (i.e. the five field approximation), the wave amplitude predicted by the analytic solution consists of a damped, oscillatory term (with respect to time) which allows the wave to propagate at approximately the speed of sound, for which the attenuation coefficient α_d is directly proportional to the shear viscosity η . The second term is non-oscillatory (evanescent) and its attenuation coefficient α_λ is directly proportional to the heat conductivity λ . Depending on the initial conditions, this system allows η and λ to be measured separately. In particular, we will show that the wave corresponding to *Case 1* propagates adiabatically (with no heat flux being present), allowing η to be measured independently. Furthermore, the heat flux q is purely evanescent (has no oscillatory contribution), such that its time evolution is completely determined by α_λ , being independent of α_d and hence of η . We will therefore use *Cases 2a* and *2b* to measure λ independently of η .

A known fundamental limitation of the first-order theory is that it allows the non-causal instantaneous response in the heat flux q and shear pressure Π induced by changes in the gradients of the fundamental variables n , β and P . In particular, this theory does not allow the values of q and Π to be set at initial time $t = 0$ independently of the values of n , β and P . This is incompatible with our initial local thermodynamic equilibrium state, in which $q = \Pi = 0$, such that the first-order theory prediction for the evolution of q and Π is not accurate for a duration of time proportional to the Anderson-Witting relaxation time τ . In the second-order hydrodynamics approach, both q and Π obey independent evolution equations which, for sufficiently small values of τ , allow them to relax from arbitrary initial configurations to the first-order predictions on time scales given by the relaxation times τ_q and τ_Π , respectively. We study these relaxation times for *Case 1* and *Case 2b* and demonstrate that $\tau_q \simeq \tau$ and $\tau_\Pi \simeq \tau$ at small values of τ .

In the analysis of *Case 2b*, we encountered a more subtle limitation of the first-order theory. If the initial state is prepared as described in *Case 2b*, the pressure perturbation δP and the shear pressure Π remain zero throughout the evolution of the wave, for all tested values of the relaxation time, provided the initial perturbation δn_0 is small. Moreover, the decay of the amplitudes of δn , β and q is strictly exponential, with no oscillations.

While the above behaviour is successfully recovered in the second-order theory, in the first-order theory, δP and Π are non-zero. Moreover, the amplitude of β is oscillatory and the oscillation amplitude is of the same order of magnitude as the non-oscillatory β predicted by the second-order theory.

Next, we consider a moment-based approach similar to the one introduced in Refs. [16, 20, 21, 28], where we expand the distribution function with respect to the Laguerre and Legendre polynomials, corresponding to the magnitude p of the particle momentum and the z component $\xi = p^z/p$ of its velocity, respectively. Retaining zeroth and first-order terms with respect to the Laguerre polynomials and terms up to second-order with respect to the Legendre polynomials, we obtain a system of 6 evolution equations for the density n , pressure P , velocity β , heat flux q , shear pressure Π and an extra non-hydrodynamic variable. In the frame of this moment-based model, we exactly recover the Chapman-Enskog predictions for the shear viscosity η and heat conductivity λ . As highlighted in Ref. [28], there is a fundamental difference between our proposed moment-based method and Grad's 14 moment approach, due to the fact that the former is based on an expansion with respect to orthogonal polynomials, while the former relies on an expansion on polynomials in p^μ , which are not orthogonal. After obtaining an analytic solution within our proposed model, we further show that, at large values of the relaxation time τ , the moment-based approach provides a better analytic description of the evolution of the heat flux compared to the second-order hydrodynamics result.

Finally, we analyse the ballistic regime, where the particle constituents stream freely. Since the flow is now collisionless, no dissipation occurs and the wave attenuation is no longer exponential. Instead, the dispersive regime sets in, since now the wave can be regarded as a packet which consists of non-interacting constituents which propagate at difference velocities ξ (this is a consequence of our convention that at initial time, the particles follow the Maxwell-Jüttner equilibrium distribution). We present an analytic solution for the linearised limit of the ballistic regime which we use to demonstrate the capability of our numerical code to capture the free-streaming dynamics.

According to Refs. [20, 21], high order quadratures (i.e. large velocity sets) are required to obtain accurate simulation results at large values of τ , when the flow is out of equilibrium and rarefaction effects become important. This is performed in a straightforward manner following the procedure described in Ref. [20] and summarised in the appendix of the present

paper. We shall therefore perform our numerical experiments using the quadrature-based R-SLB models developed in Ref. [20]. While the analysis presented herein is restricted to the case of massless particles, it can be easily extended to the case of massive particles, e.g. following Refs. [22, 23, 29].

The paper is organised as follows. The general framework for the study of the propagation of longitudinal waves is introduced in Sec. II by linearising the relativistic hydrodynamic equations with respect to the wave amplitude. The relativistic Boltzmann equation in the Anderson-Witting approximation for the collision term (the AWB equation) is also briefly presented, alongside a description of the Landau frame. In Secs. III and IV, we consider the longitudinal wave problem from the perspective of the first-order and second order hydrodynamics theories, respectively, while in Sec. V, we consider a moment-based approach. In all cases, we rely on numerical simulations to study the validity and applicability of these theories as the relaxation time is increased. In Sec. VI, we analyse analytically and numerically the propagation of the longitudinal wave in the ballistic regime, where the attenuation is dispersive rather than dissipative. A short description of the numerical method employed in this paper is provided in Appendix A.

Throughout this paper, we use the metric convention $\eta_{\mu\nu} = \text{diag}(-1, 1, 1, 1)$ and Planck units, such that $c = \hbar = K_B = 1$.

II. RELATIVISTIC FLUID DYNAMICS

In this section, we present the common framework used in later sections for the analysis of the evolution of longitudinal waves. In Subsec. II A, we briefly review the connection between the relativistic Boltzmann equation and the macroscopic hydrodynamic equations, which are written in linearised form in Subsec. II B. The equations which serve as the basis for the analysis of longitudinal waves are presented in Subsec. II C.

A. Relativistic kinetic theory

In this paper, we will focus on the relativistic Boltzmann equation for massless particles in the Anderson-Witting approximation for the collision term [3]:

$$p^\mu \partial_\mu f = \frac{p \cdot u_L}{\tau} (f - f_L^{(\text{eq})}), \quad (2.1)$$

where we assume for simplicity that the relaxation time τ is constant. The equilibrium distribution $f^{(\text{eq})}$ is taken to be the Maxwell-Jüttner distribution function:

$$f_L^{(\text{eq})} = \frac{n_L}{8\pi T_L^3} \exp\left(\frac{p \cdot u_L}{T_L}\right). \quad (2.2)$$

In the above, n_L represents the particle number density, u_L^μ is the macroscopic four-velocity, T_L is the local temperature and p^μ is the on-shell particle four-momentum. The quantities bearing the subscript L are expressed in the Landau (energy) frame [3, 30].

The transition from the Boltzmann equation (2.1) to relativistic hydrodynamics is done by considering the macroscopic four-flow vector N^μ and stress-energy tensor (SET) $T^{\mu\nu}$, which are obtained by integrating the distribution function over the momentum space:

$$N^\mu = \int \frac{d^3p}{p^0} f p^\mu, \quad T^{\mu\nu} = \int \frac{d^3p}{p^0} f p^\mu p^\nu. \quad (2.3)$$

Substituting $f_L^{(\text{eq})}$ (2.2) into Eq. (2.3) gives the equilibrium four-flow vector $N_{(\text{eq})}^\mu$ and SET $T_{(\text{eq})}^{\mu\nu}$:

$$N_{(\text{eq})}^\mu = n_L u_L^\mu, \quad T_{(\text{eq})}^{\mu\nu} = (E_L + P_L) u_L^\mu u_L^\nu + P_L \eta^{\mu\nu}. \quad (2.4)$$

The Landau velocity u_L^μ is defined as the eigenvector of $T^{\mu\nu}$ corresponding to the Landau energy density E_L :

$$T^\mu{}_\nu u_L^\nu = -E_L u_L^\mu. \quad (2.5)$$

For massless particles, $E_L = 3P_L$ and the Landau pressure $P_L = n_L T_L$ is used to define the Landau temperature T_L , while the Landau particle number density n_L is obtained by contracting N^μ with u_L^μ :

$$n_L = -N_\mu u_L^\mu. \quad (2.6)$$

Multiplying the Boltzmann equation (2.1) by the collision invariants $\psi \in \{1, p^\mu\}$ and integrating with respect to the momentum space, the following conservation equations are obtained:

$$\partial_\mu N^\mu = 0, \quad \partial_\nu T^{\mu\nu} = 0. \quad (2.7)$$

Due to its simplicity and pedagogical value, we will work in this paper in the Eckart (particle) frame, where the macroscopic velocity u^μ is defined as the unit vector parallel to N^μ [31, 32]:

$$u^\mu = N^\mu / \sqrt{-N^2}. \quad (2.8)$$

With respect to u^μ , N^μ and the (SET) $T^{\mu\nu}$ can be decomposed as:

$$N^\mu = nu^\mu, \quad T^{\mu\nu} = Eu^\mu u^\nu + (P + \bar{\omega})\Delta^{\mu\nu} + u^\mu q^\nu + q^\nu u^\mu + \Pi^{\mu\nu}, \quad (2.9)$$

where $\Delta^{\mu\nu} = \eta^{\mu\nu} + u^\mu u^\nu$ is the projector on the hypersurface orthogonal to u^μ . The particle number density n , energy density E , isotropic pressure $P + \bar{\omega}$, heat flux q^μ and shear stress tensor $\Pi^{\mu\nu}$ can be obtained as follows [27, 32]:

$$\begin{aligned} n &= -u_\mu N^\mu, & E &= u_\mu u_\nu T^{\mu\nu}, & P &= \frac{1}{3}\Delta_{\mu\nu} T^{\mu\nu}, \\ \Pi^{\mu\nu} &= \left(\Delta^\mu{}_\lambda \Delta^\nu{}_\kappa - \frac{1}{3}\Delta^{\mu\nu} \Delta_{\lambda\kappa} \right) T^{\lambda\kappa}, \\ q^\mu &= -\Delta^\mu{}_\nu u_\lambda T^{\nu\lambda}, \end{aligned} \quad (2.10)$$

while the dynamic pressure $\bar{\omega} = 0$ for massless particles, when $E = 3P$. In general, the Eckart quantities introduced above are different from the corresponding quantities defined in the Landau frame (more details will be given in Sec. II B).

The system (2.7) consisting of 5 equations is not closed, since q^μ and $\Pi^{\mu\nu}$ are *a priori* unconstrained. The constitutive relations corresponding to the first- and second-order relativistic hydrodynamics frameworks will be discussed in Secs. III and IV.

B. Linearised relativistic hydrodynamics

We now consider a system which is homogeneous along the x and y directions. In this case, the AWB equation (2.1) reduces to [20]:

$$\partial_t f + \xi \partial_z f = -\frac{\gamma_L(1 - \beta_L \xi)}{\tau}(f - f_L^{(\text{eq})}), \quad f_L^{(\text{eq})} = \frac{n_L}{8\pi T_L^3} \exp \left[-\frac{p\gamma_L}{T_L}(1 - \beta_L \xi) \right], \quad (2.11)$$

where $\xi = p^z/p$ represents the particle velocity along the z axis, taking values in $[-1, 1]$. Taking into account the constraints $u_\mu q^\mu = 0$ and $u_\mu \Pi^{\mu\nu} = 0$, the variables u^μ , q^μ and $\Pi^{\mu\nu}$ can be taken as follows [20, 27]:

$$\begin{aligned} u &= \gamma(\partial_t + \beta \partial_z), & q &= q(\beta \partial_t + \partial_z), \\ \Pi^{\mu\nu} &= \Pi \begin{pmatrix} \beta^2 \gamma^2 & 0 & 0 & \beta \gamma^2 \\ 0 & -\frac{1}{2} & 0 & 0 \\ 0 & 0 & -\frac{1}{2} & 0 \\ \beta \gamma^2 & 0 & 0 & \gamma^2 \end{pmatrix}, \end{aligned} \quad (2.12)$$

where $\gamma = (1 - \beta^2)^{-1/2}$ is the Lorentz factor corresponding to the velocity β . The Landau frame can be constructed analytically by solving the eigenvalue equation (2.5) [20, 27]:

$$\begin{aligned} E_L &= \frac{1}{2} \left[T^{00} - T^{zz} + \sqrt{(T^{00} + T^{zz})^2 - 4(T^{0z})^2} \right], \\ \beta_L &= \frac{T^{0z}}{E + T^{zz}}. \end{aligned} \quad (2.13)$$

In order to arrive at the linearised form of Eqs. (2.7), we consider that $\beta \ll 1$, while n and P can be written as:

$$n = n_0 + \delta n, \quad P = P_0 + \delta P, \quad (2.14)$$

where $\delta n/n_0$ and $\delta P/P_0$ are quantities of order $O(\beta)$. Furthermore, we will consider that Π and q are also of order $O(\beta)$, since they represent non-equilibrium quantities. Neglecting the terms of order β^2 , N^μ and $T^{\mu\nu}$ (2.9) reduce to:

$$\begin{aligned} N^\mu &\simeq (n_0 + \delta n, 0, 0, n_0 \beta)^T, \\ T^{\mu\nu} &\simeq \begin{pmatrix} 3(P_0 + \delta P) & 0 & 0 & 4\beta P_0 + q \\ 0 & P_0 + \delta P - \frac{\Pi}{2} & 0 & 0 \\ 0 & 0 & P_0 + \delta P - \frac{\Pi}{2} & 0 \\ 4\beta P_0 + q & 0 & 0 & P_0 + \delta P + \Pi \end{pmatrix}, \end{aligned} \quad (2.15)$$

while the Landau quantities n_L , P_L and β_L can be approximated through:

$$n_L \simeq n_0 + \delta n, \quad P_L \simeq P_0 + \delta P, \quad \beta_L \simeq \beta + \frac{q}{4P_0}. \quad (2.16)$$

In the linearised approximation, the conservation equations (2.7) reduce to:

$$\begin{aligned} \partial_t \delta n + n_0 \partial_z \beta &= 0, \\ 3\partial_t \delta P + 4P_0 \partial_z \beta + \partial_z q &= 0, \\ 4P_0 \partial_t \beta + \partial_t q + \partial_z \delta P + \partial_z \Pi &= 0. \end{aligned} \quad (2.17)$$

Noting that $f - f_L^{(\text{eq})}$ is also of order $O(\beta)$, the Boltzmann equation (2.11) can also be expressed in linearised form:

$$\partial_t f + \xi \partial_z f \simeq -\frac{1}{\tau} (f - f_L^{(\text{eq})}), \quad (2.18)$$

where $f_L^{(\text{eq})}$ can be linearised as follows:

$$f_L^{(\text{eq})} \simeq \frac{n_0}{8\pi T_0^3} e^{-p/T_0} \left[1 + \frac{p\xi}{T_0} \left(\beta + \frac{q}{4P_0} \right) + \frac{4\delta n}{n_0} - \frac{3\delta P}{P_0} + \frac{p}{T_0} \left(\frac{\delta P}{P_0} - \frac{\delta n}{n_0} \right) \right]. \quad (2.19)$$

C. Longitudinal waves

We now seek solutions of the form:

$$\begin{pmatrix} \beta \\ q \end{pmatrix} = \begin{pmatrix} \widetilde{\beta} \\ \widetilde{q} \end{pmatrix} \sin kz, \quad \begin{pmatrix} \delta n \\ \delta P \\ \Pi \end{pmatrix} = \begin{pmatrix} \widetilde{\delta n} \\ \widetilde{\delta P_\alpha} \\ \widetilde{\Pi_\alpha} \end{pmatrix} \cos kz, \quad (2.20)$$

where $k = 2\pi/L$ is the wave number and L is the wavelength. The quantities with a tilde $\widetilde{M} \in \{\widetilde{\beta}, \widetilde{\delta n}, \widetilde{\delta P}, \widetilde{q}, \widetilde{\Pi}\}$ depend only on time t . Taking this dependence in the form:

$$\widetilde{M} = \sum_{\alpha} M_{\alpha} e^{-\alpha t}, \quad (2.21)$$

Eq. (2.17) can be solved for each (constant) value of α independently, yielding a spectrum of linearly-independent modes satisfying:

$$\alpha \delta n_{\alpha} - k n_0 \beta_{\alpha} = 0, \quad (2.22a)$$

$$3\alpha \delta P_{\alpha} - 4k P_0 \beta_{\alpha} - k q_{\alpha} = 0, \quad (2.22b)$$

$$4\alpha P_0 \beta_{\alpha} + \alpha q_{\alpha} + k \delta P_{\alpha} + k \Pi_{\alpha} = 0. \quad (2.22c)$$

The imaginary part of α represents the propagation angular frequency, while its real part causes the dissipative dampening of the wave. In order to solve the above set of equations, the constitutive equations for q and Π must be supplied separately.

The initial conditions for Eqs. (2.22) are given in the form

$$\widetilde{\beta}(t=0) = \beta_0, \quad \widetilde{\delta n}(t=0) = \delta n_0, \quad \widetilde{\delta P}(t=0) = \delta P_0. \quad (2.23)$$

In this paper, we consider the following sets of values for β_0 , δn_0 and δP_0 :

- *Case 1:* $\delta n_0 = \delta P_0 = 0$, $\beta_0 \neq 0$;
- *Case 2a:* $\delta n_0 = \beta_0 = 0$, $\delta P_0 \neq 0$;
- *Case 2b:* $\beta_0 = \delta P_0 = 0$, $\delta n_0 \neq 0$.

In Secs. III and IV, we will employ the constitutive relations corresponding to the first- and second-order relativistic hydrodynamics. In Sec. V we will construct a solution of Eqs. (2.22) starting from the Boltzmann equation (2.18) written in linearised form.

III. FIRST ORDER HYDRODYNAMICS

The equations of first order relativistic hydrodynamics represent the analogue of the Navier-Stokes-Fourier equations of non-relativistic hydrodynamics. In this formulation, the fields n , u^μ and P are considered as fundamental variables. Since u^μ is normalised according to $u^2 = -1$, the theory contains five independent fields and is sometimes referred to as the five field theory [1]. In this first order framework, the constitutive equations for the heat flux q^μ and shear stress tensor $\Pi^{\mu\nu}$ represent algebraic relations linking them to the gradients of the fundamental fields via the transport coefficients λ (heat conductivity) and η (shear viscosity), respectively. Since q^μ and $\Pi^{\mu\nu}$ respond instantaneously to changes in the fundamental fields, the ensuing system of equations is not hyperbolic [32], rendering the theory non-causal. This issue can be remedied within the second order relativistic hydrodynamics framework, as will be discussed in Sec. IV. In this section, we will focus on determining λ and η by comparing the analytical and numerical results for the attenuation process occurring in the longitudinal wave problem described in Sec. II C.

A. Constitutive relations

The constitutive equations for q^μ and $\Pi^{\mu\nu}$ can be written in the frame of the first-order relativistic hydrodynamics as [1, 32]:

$$\begin{aligned} q^\mu &= -\lambda \Delta^{\mu\nu} \left(\partial_\nu T - \frac{T}{E + P} \partial_\nu P \right), \\ \Pi^{\mu\nu} &= -2\eta \left[\frac{1}{2} (\Delta^{\mu\lambda} \Delta^{\nu\kappa} + \Delta^{\nu\lambda} \Delta^{\mu\kappa}) - \frac{1}{3} \Delta^{\mu\nu} \Delta^{\lambda\kappa} \right] \partial_\lambda u_\kappa, \end{aligned} \quad (3.1)$$

where λ and η represent the coefficients of heat conductivity and shear viscosity η , respectively. At the level of the first-order hydrodynamics theory, it is not specified whether the macroscopic velocity u^μ appearing in the right hand side of the second line of Eq. (3.1) is defined in the Eckart or in the Landau frame. In this section, we will consider the Landau frame velocity, since this choice seems natural when the Anderson-Witting approximation is used for the collision term [11–13, 27, 28, 36–38, 40]. In Sec. V, we will show that this choice arises naturally when a moment-based approach is used to solve the AWB equation (2.18).

The connection between the Boltzmann equation (2.1) and the constitutive equations

(3.1) is commonly achieved via two paths: (a) the Chapman-Enskog expansion; and (b) Grad's 14 moments approximation. In the ultrarelativistic regime considered in this paper, the transport coefficients η and λ are given by:

$$\eta = \eta_0 P \tau, \quad \lambda = \lambda_0 n \tau, \quad (3.2)$$

where the dimensionless constants η_0 and λ_0 are obtained using Grad's approximation and the Chapman-Enskog procedure as follows [1]:

$$\text{Grad method:} \quad \eta_{0,G} = \frac{2}{3}, \quad \lambda_{0,G} = \frac{4}{5}, \quad (3.3a)$$

$$\text{Chapman-Enskog :} \quad \eta_{0,C-E} = \frac{4}{5}, \quad \lambda_{0,C-E} = \frac{4}{3}. \quad (3.3b)$$

The validity of the constitutive equations (3.1) and of the above expressions for the transport coefficients is limited to the hydrodynamic regime, i.e. when the relaxation time τ is sufficiently small.

In the linearised approximation introduced in Sec. II B, the constitutive equations (3.1) reduce to:

$$q = -\frac{\lambda P_0}{4n_0} \left(\frac{3}{P_0} \partial_z \delta P - \frac{4}{n_0} \partial_z \delta n \right), \quad \Pi = -\frac{4\eta}{3} \partial_z \left(\beta + \frac{q}{4P_0} \right), \quad (3.4)$$

where $u_L^\mu \simeq (1, 0, 0, \beta + q/4P_0)$ was used in the expression for Π .

B. Longitudinal waves solution

The modes q_α and Π_α appearing in Eq. (2.22) can be found from Eq. (3.4):

$$q_\alpha = \frac{k\lambda P_0}{4n_0} \left(3 \frac{\delta P_\alpha}{P_0} - 4 \frac{\delta n_\alpha}{n_0} \right), \quad \Pi_\alpha = -\frac{4k\eta}{3} \left(\beta_\alpha + \frac{q_\alpha}{4P_0} \right). \quad (3.5)$$

Noting from Eq. (2.22a) that

$$\frac{\delta n_\alpha}{n_0} = \frac{k}{\alpha} \beta_\alpha, \quad (3.6)$$

Eq. (2.22b) reduces to:

$$P_0 \left(3 \frac{\delta P_\alpha}{P_0} - 4 \frac{\delta n_\alpha}{n_0} \right) \left(\frac{\lambda k^2}{4n_0} - \alpha \right) = 0. \quad (3.7)$$

According to Eq. (3.5), the first parenthesis vanishes only when $q_\alpha = 0$. Thus, the solution

$$\alpha_\lambda = \frac{k^2 \lambda}{4n_0} \quad (3.8)$$

corresponds to the only mode which dissipates heat. In this case, Eq. (2.22) can be used to obtain:

$$\delta n_\lambda = \frac{kn_0}{\alpha_\lambda} \beta_\lambda, \quad \delta P_\lambda = 0, \quad q_\lambda = -4P_0 \beta_\lambda, \quad \Pi_\lambda = 0. \quad (3.9)$$

It is remarkable that this mode induces no viscous dissipation.

Considering now that $q = 0$, Eq. (2.22c) reduces to:

$$4P_0 \beta_\alpha \left(\alpha + \frac{k^2}{3\alpha} - \frac{k^2 \eta}{3P_0} \right) = 0. \quad (3.10)$$

The solution $\beta_\alpha = 0$ is trivial since in this case $\delta n_\alpha = \delta P_\alpha = 0$. Setting the quantity inside the parenthesis equal to zero yields the following allowed values for α :

$$\alpha_\pm = \alpha_d \pm i\alpha_o, \quad (3.11)$$

where the dampening (α_d) and oscillatory (α_o) parts of α_\pm read:

$$\alpha_d = \frac{k^2 \eta}{6P_0}, \quad \alpha_o = \frac{k}{\sqrt{3}} \sqrt{1 - \frac{3\alpha_d^2}{k^2}}, \quad (3.12)$$

It is worth noting that the phase velocity $\alpha_o/k = c_s \sqrt{1 - \frac{3\alpha_d^2}{k^2}}$ predicted in the first order theory is smaller than the sound speed $c_s = 1/\sqrt{3}$. The amplitudes of the density and pressure perturbations δn_\pm and δP_\pm are given in terms of the velocity amplitudes β_\pm as follows:

$$\delta n_\pm = \frac{kn_0}{\alpha_\pm} \beta_\pm, \quad \delta P_\pm = \frac{4kP_0}{3\alpha_\pm} \beta_\pm. \quad (3.13)$$

Taking into account the above allowed values for α , the general solution (2.21) reads:

$$\begin{pmatrix} \tilde{\beta} \\ \tilde{\delta n} \\ \tilde{\delta P} \\ \tilde{q} \\ \tilde{\Pi} \end{pmatrix} = \begin{pmatrix} \beta_\lambda \\ \delta n_\lambda \\ 0 \\ q_\lambda \\ 0 \end{pmatrix} e^{-\alpha_\lambda t} + \left[\begin{pmatrix} \beta_c \\ \delta n_c \\ \delta P_c \\ 0 \\ \Pi_c \end{pmatrix} \cos \alpha_o t + \begin{pmatrix} \beta_s \\ \delta n_s \\ \delta P_s \\ 0 \\ \Pi_s \end{pmatrix} \sin \alpha_o t \right] e^{-\alpha_d t}. \quad (3.14)$$

In the above, β_λ , $\beta_c = \beta_+ + \beta_-$ and $\beta_s = -i(\beta_+ - \beta_-)$ are independent integration constants

with respect to which we have defined:

$$\begin{aligned}\begin{pmatrix} \delta n_c \\ \delta P_c \end{pmatrix} &= \begin{pmatrix} kn_0 \\ 4kP_0/3 \end{pmatrix} \frac{\alpha_d \beta_c + \alpha_o \beta_s}{\alpha_d^2 + \alpha_o^2}, \\ \begin{pmatrix} \delta n_s \\ \delta P_s \end{pmatrix} &= \begin{pmatrix} kn_0 \\ 4kP_0/3 \end{pmatrix} \frac{\alpha_d \beta_s - \alpha_o \beta_c}{\alpha_d^2 + \alpha_o^2}, \\ \begin{pmatrix} \Pi_c \\ \Pi_s \end{pmatrix} &= -\frac{8\alpha_d P_0}{k} \begin{pmatrix} \beta_c \\ \beta_s \end{pmatrix},\end{aligned}\tag{3.15}$$

while $q_c = q_s = 0$. The other constants δn_λ , δP_λ , Π_λ and q_λ were already defined in Eq. (3.9).

The constants β_λ , β_c and β_s can be obtained by substituting the solution (3.14) into the initial conditions (2.23) yielding:

$$\beta_\lambda + \beta_c = \beta_0, \quad \delta n_\lambda + \delta n_c = \delta n_0, \quad \delta P_c = \delta P_0.\tag{3.16}$$

The solution of Eq. (3.16) can be written as:

$$\begin{aligned}\beta_\lambda &= \frac{\alpha_\lambda}{4k} \left(\frac{4\delta n_0}{n_0} - \frac{3\delta P_0}{P_0} \right), \\ \beta_c &= \beta_0 - \frac{\alpha_\lambda}{4k} \left(\frac{4\delta n_0}{n_0} - \frac{3\delta P_0}{P_0} \right), \\ \beta_s &= -\frac{\alpha_d}{\alpha_o} \beta_0 + \frac{\alpha_\lambda \alpha_d}{k \alpha_o} \frac{\delta n_0}{n_0} + \frac{3\delta P_0}{4k P_0 \alpha_o} (\alpha_d^2 + \alpha_o^2 - \alpha_\lambda \alpha_d).\end{aligned}\tag{3.17}$$

The analytic solution presented in this section facilitates the study of the transport coefficients corresponding to a relativistic gas. Using the numerical method described in Appendix A, we will consider this system in the following subsection for the study of the ultrarelativistic limits of the shear viscosity η and heat conductivity λ arising from the AWB equation (2.1).

C. Case 1: Adiabatic flow

First, we consider an adiabatic flow (i.e. $q = 0$) such that the shear viscosity η can be isolated from the heat conductivity λ . This can be achieved when $3n_0\delta P_0 = 4P_0\delta n_0$. This condition is equivalent to the requirement that the fugacity $\lambda_{\text{fug}} = n^4/P^3$ is constant in the initial state. Indeed, combining the first two relations in Eq. (2.17) gives:

$$\partial_t \delta \lambda + \partial_z (q/P_0) = 0.\tag{3.18}$$

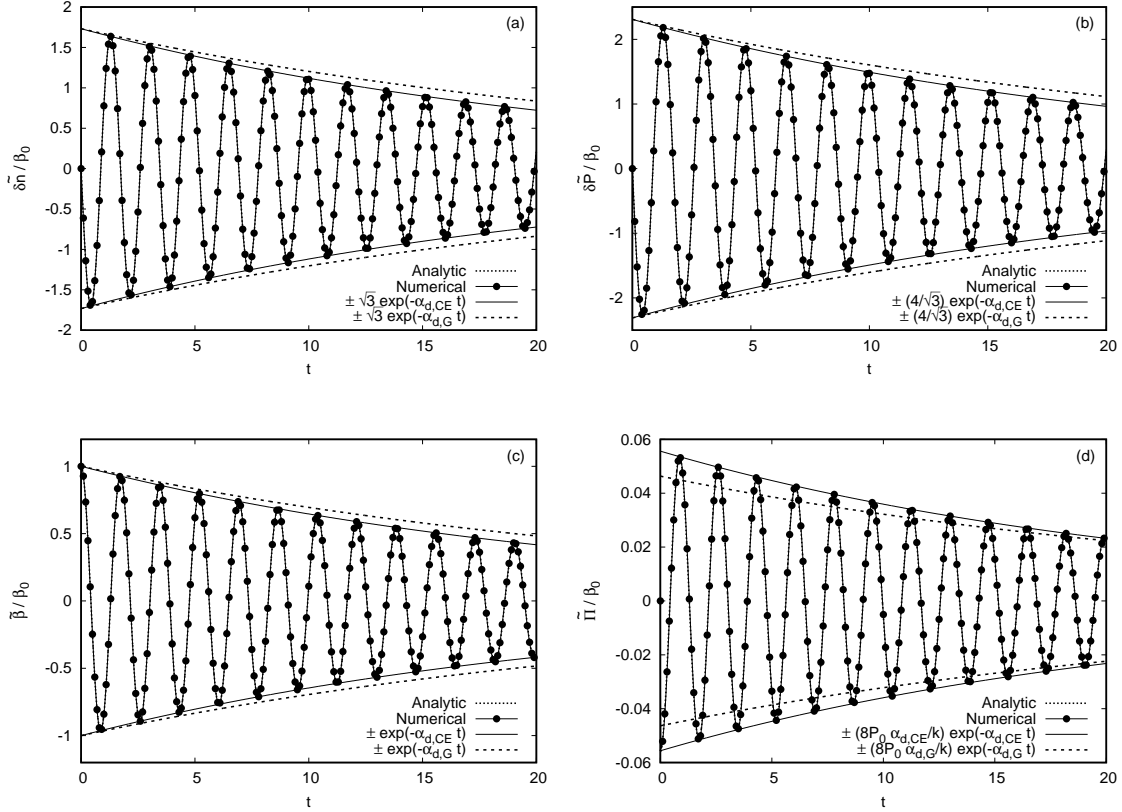


FIG. 1. Comparison between the analytic solutions in Eq. (3.20) corresponding to the Chapman-Enskog value for η (continuous lines) and numerical results (dotted lines and points) for $\tau = 8.3 \times 10^{-3}$. The vertical axes represent the values of (a) $\widetilde{\delta n}$, (b) $\widetilde{\delta P}$, (c) $\widetilde{\beta}$ and (d) $\widetilde{\Pi}$, divided by β_0 . The coefficients $\alpha_{d,CE}$ and $\alpha_{d,G}$ in the asymptotic dampening lines are obtained from Eq. (3.12) by substituting the Chapman-Enskog (3.3b) and Grad (3.3a) expressions for η . The system was initialised according to *Case 1*, i.e. $\delta n_0 = \delta P_0 = 0$ and $\beta_0 = 10^{-3}$.

The above equation (valid in the linearised regime) shows that if there is no heat flux present, the fugacity remains constant in time.

We further note that Eq. (3.17) indicates that $\beta_\lambda = 0$ when $3n_0\delta P_0 = 4P_0\delta n_0$, while Eq. (3.9) implies that δn_λ , δP_λ , q_λ and Π_λ cancel. Thus, the evolution of the fluid is completely independent of α_λ , enabling η to be determined independently. For simplicity, we will consider the initialisation corresponding to *Case 1* in Sec. II C, according to which $\delta n_0 = \delta P_0 = 0$. In this limit, Eqs. (3.17) reduce to:

$$\beta_c = \beta_0, \quad \beta_s = -\frac{\alpha_d}{\alpha_o}\beta_0, \quad \beta_\lambda = 0, \quad (3.19)$$

such that the exact solution (3.14) reads:

$$\begin{aligned} \begin{pmatrix} \tilde{\beta} \\ \tilde{\Pi} \end{pmatrix} &= \beta_0 \begin{pmatrix} 1 \\ -8P_0\alpha_d/k \end{pmatrix} \left(\cos \alpha_o t - \frac{\alpha_d}{\alpha_o} \sin \alpha_o t \right) e^{-\alpha_d t}, \\ \widetilde{\delta n} &= -\frac{kn_0\beta_0}{\alpha_o} e^{-\alpha_d t} \sin \alpha_o t, \\ \widetilde{\delta P} &= -\frac{4kP_0\beta_0}{3\alpha_o} e^{-\alpha_d t} \sin \alpha_o t, \end{aligned} \quad (3.20)$$

where α_d and α_o are given in terms of η in Eq. (3.12).

The analytic results in Eq. (3.20) are represented in Fig. 1 for the initial conditions $\beta_0 = 10^{-3}$ and $\delta n_0 = \delta P_0 = 0$ alongside the corresponding numerical results obtained using the method described in Appendix A. The relaxation time was taken to be $\tau = 0.0083$, such that both the dampening and the oscillatory characteristics of the solutions can be highlighted on the same timescale. The first entry in the legend (fine dotted lines) corresponds to the analytic expressions in Eqs. (3.20), where α_d and α_o are computed using the Chapman-Enskog value for η . The numerical results are indistinguishable from the analytic predictions.

Also in the plots in Fig. 1, the dampening caused by the $\exp(-\alpha_d t)$ factor in Eqs. (3.20) is represented when α_d is calculated using the Chapman-Enskog and Grad expressions for η . In the amplitude of the dampening terms in $\tilde{\beta}/\beta_0$ and $\tilde{\Pi}/\beta_0$, we have used the approximation $\sqrt{1 + \alpha_d^2/\alpha_o^2} \simeq 1$. It can be seen that the dampening predicted by the analytic solution when the Grad expression for η is used does not match the numerical results.

D. Cases 2a and 2b: Non-adiabatic flow

The coefficient α_λ can be investigated most easily by considering the decay of the amplitude \tilde{q} of the heat flux. To this end, we will consider the initialisations corresponding to *Case 2a* ($\delta n_0 = \beta_0 = 0$ and $\delta P_0 = 10^{-3}$) and *Case 2b* ($\delta P_0 = \beta_0 = 0$ and $\delta n_0 = 10^{-3}$) described in Sec. II C. According to Eqs. (3.9) and (3.17), \tilde{q} takes the following form:

$$\tilde{q} = \frac{\alpha_\lambda P_0}{k} \left(\frac{3\delta P_0}{P_0} - \frac{4\delta n_0}{n_0} \right) e^{-\alpha_\lambda t}. \quad (3.21)$$

The above analytic result is compared in Fig. 2 to the numerical results obtained using the method described in Appendix A. For each of the two cases mentioned above, three curves are represented. Our numerical results (dashed lines and points) are overlapped with the analytic prediction (3.21) when α_λ is calculated using the Chapman-Enskog expression

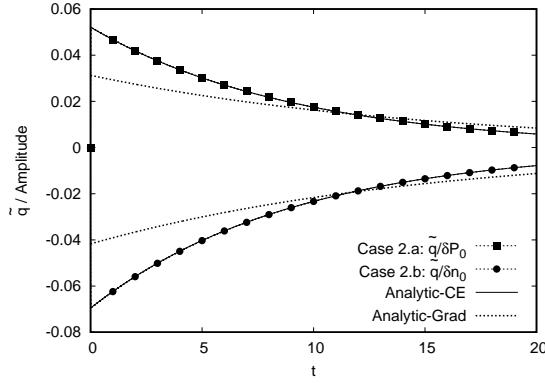


FIG. 2. The time evolution of \tilde{q} for the initialisations corresponding to *Case 2 (a)* (i.e. $\delta n_0 = \beta_0 = 0$ and $\delta P_0 = 10^{-3}$) and *Case 2 (b)* (i.e. $\delta P_0 = \beta_0 = 0$ and $\delta n_0 = 10^{-3}$). The dotted lines with points represent the numerical results. The analytic solution (3.21) is represented for the two cases using solid lines when α_λ is computed using the Chapman-Enskog expression for λ (3.3b), while the dotted lines correspond to the case when the Grad expression (3.3a) is used. The relaxation time was set to $\tau = 0.0083$.

for λ (continuous line). The analytic prediction (3.21) corresponding to the case when α_λ is obtained using the Grad expression for λ (dashed line) is clearly not consistent with our numerical results. The points at $t = 0$ indicate that in the numerical simulations, the system was initialised using an equilibrium state, in which the heat flux vanishes. In the five-field theory, the initial value of \tilde{q} does not represent a free parameter, as can be seen from the solution in Eq. (3.21). However, since τ is small, the system quickly relaxes towards the five-field theory prediction (3.21). We will further consider this relaxation process in Sec. IV.

E. Limits of the linearised hydrodynamics equations

We now test the limits within which the solution of the linearised equations (2.17) are applicable. In order to reduce the rarefaction effects, we fix $\tau = 0.0083$ throughout this subsection.

The solution (3.20) predicts that, for *Case 1*, the time evolution of $\tilde{\beta}$ is damped according to the factor $\exp(-\alpha_d t)$, with α_d (3.12) being independent of the magnitude β_0 of the perturbation. Figure 3 shows that this is not the case: while at small values of β_0 , $\tilde{\beta}$

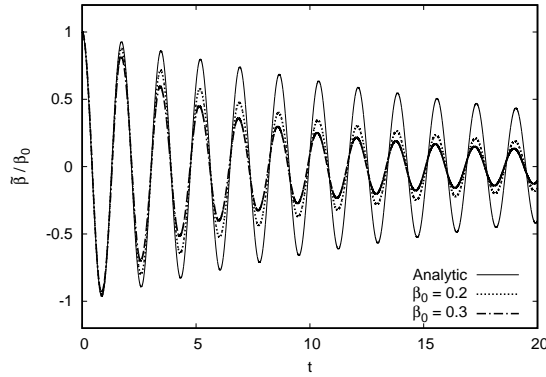


FIG. 3. The ratio $\tilde{\beta}/\beta_0$ for various values of β_0 corresponding to *Case 1* presented in Sec. II C. As β_0 increases, the time evolution of $\tilde{\beta}/\beta_0$ departs from the solution (3.20), indicating that nonlinear effects become important.

follows closely the analytic prediction [as confirmed in Fig. 1(c)], at larger values of β , the dampening is enhanced compared to the linearised limit (3.12). Indeed, the dampening of $\tilde{\beta}$ is stronger when $\beta_0 = 0.3$ than when $\beta_0 = 0.2$, which in turn is stronger than in the linearised regime.

In order to test the versatility of the functional form of the solution corresponding to the linearised regime, the parameters α_d , α_o and α_λ are determined using nonlinear fits of the analytic solutions (3.20) and (3.21) to the corresponding numerical data. The coefficients α_d and α_o are obtained using a two-parameter nonlinear fit of $\tilde{\delta n}$, $\tilde{\beta}$, $\tilde{\delta P}$ and $\tilde{\Pi}$ given in Eq. (3.20) for the initial conditions corresponding to *Case 1* (i.e. $\delta n_0 = \delta P_0 = 0$ and various values of β_0) to the corresponding numerical results. The coefficient α_λ is obtained by performing a one-parameter nonlinear fit of \tilde{q} with the initial conditions described in *Case 2a* ($\beta_0 = 0$, $\delta n_0 = 0$ and various values for δP_0) and *Case 2b* ($\beta_0 = 0$, $\delta P_0 = 0$ and various values for δn_0).

The dependence of α_d , α_o and α_λ on the amplitude of the perturbations is presented in the plots (a), (b) and (c) of Fig. 4, respectively. The horizontal axis in Fig. 4(c) represents the amplitude of the initial perturbation, i.e. δP_0 for *Case 2a* and δn_0 for *Case 2b*. All of the above plots show the analytic predictions (3.12) and (3.8) for α_d , α_o and α_λ , specialised to the cases when the transport coefficients η and λ are computed using the Chapman-Enskog (3.3b) and the Grad (3.3a) expressions. The results clearly favour the Chapman-Enskog

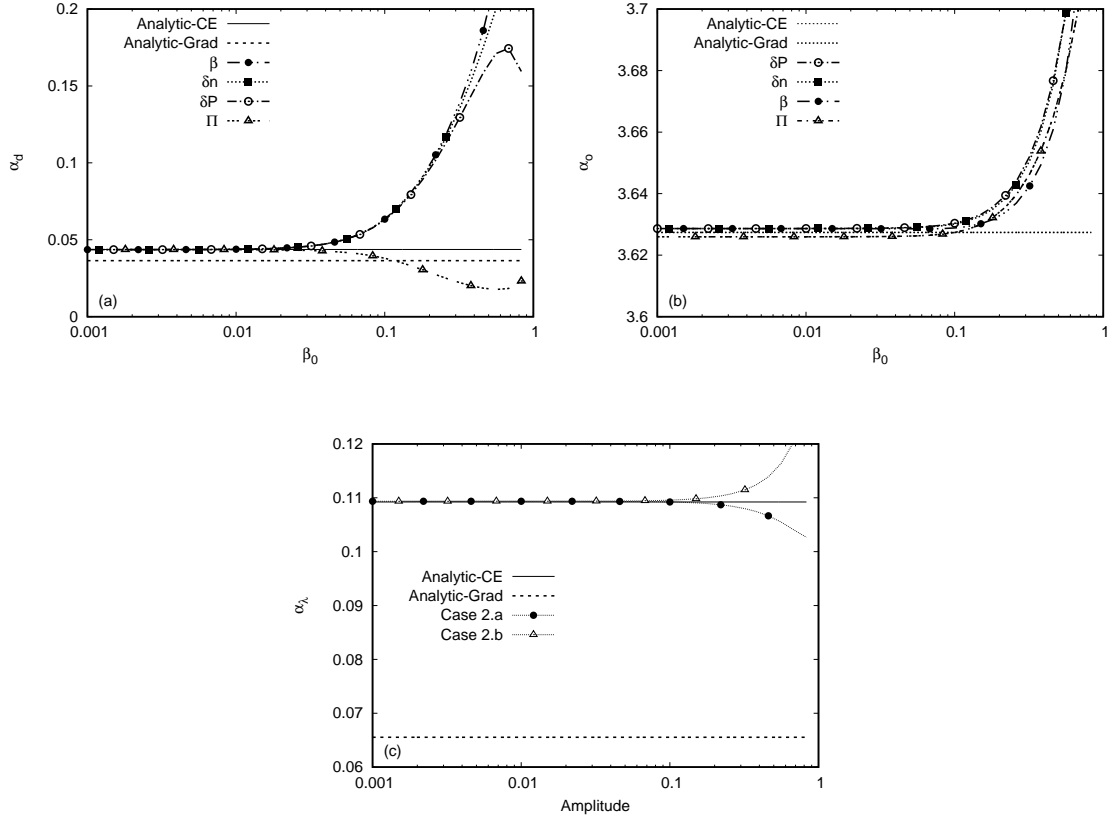


FIG. 4. The dependence of (a) α_d and (b) α_o on β_0 ; the four curves correspond to the two-parameter nonlinear fits of $\widetilde{\delta n}$, $\widetilde{\delta P}$, $\widetilde{\beta}$ and $\widetilde{\Pi}$ in Eq. (3.20) to the corresponding numerical data, as described in Subsec. III E. (c) The dependence of α_λ , obtained using a nonlinear fit of Eq. (3.21) to the numerical data, on the amplitudes δP_0 (*Case 2a*) and δn_0 (*Case 2b*) of the initial perturbation. The relaxation time was always kept at $\tau = 0.0083$.

expressions. It is also evident from these plots that the analytic analysis performed in Sec. III B in the context of the linearised hydrodynamic equations loses applicability when the perturbation amplitudes β_0 , $\delta n_0/n_0$ or $\delta P_0/P_0$ are larger than ~ 0.1 .

F. Limits of the hydrodynamic regime

It is known that the constitutive equations (2.7) are valid only when τ is small [1]. In this subsection, we focus on the validity of the analysis presented in Sec. III B as the relaxation time τ is increased.

In order to test the effect of increasing τ , we keep the perturbations small, i.e. $\beta_0 = 10^{-3}$

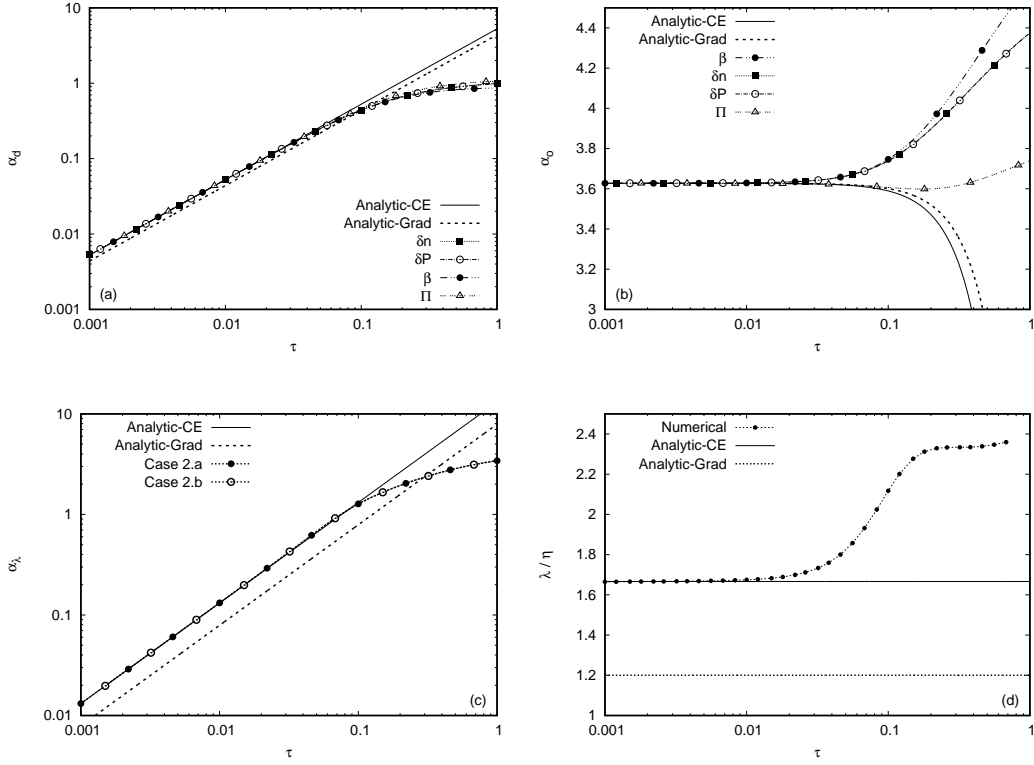


FIG. 5. Graphical representation of the dependence on τ of (a) α_d , (b) α_o and (c) α_λ obtained using the nonlinear fitting procedure described in Subsec. III E. In (d), the ratio α_λ/α_d is represented with respect to τ , where α_d is obtained using the two-parameter nonlinear fit of $\tilde{\beta}$ (3.20) on the numerical data, while α_λ is obtained using a one-parameter nonlinear fit of \tilde{q} (3.21) for *Case 2a*. The perturbation amplitude is in all cases set to 10^{-3} . On each plot, the analytic curves corresponding to the Chapman-Enskog and Grad methods are displayed.

(for *Case 1*), $\delta P_0 = 10^{-3}$ (for *Case 2a*), or $\delta n_0 = 10^{-3}$ (for *Case 2b*). The plots in Fig. 5 show the dependence of (a) α_d , (b) α_o , (c) α_λ and (d) the ratio $\lambda/\eta = 2\alpha_\lambda n_0/3\alpha_d P_0$ on the value of τ . As before, the analytic predictions for the dependence of these coefficients on τ is also shown for the cases when the transport coefficients η and λ are obtained using the Chapman-Enskog (3.3b) and Grad (3.3a) expressions. For $\tau < 0.1$, our numerical results clearly favour the Chapman-Enskog expression. Plot (d) confirms that for small values of τ , the ratio λ/η is equal to $5/3$, as predicted in the Chapman-Enskog theory (3.3b). This value is in agreement with the high chemical potential limit of Fig. 2 in Ref. [38].

While for $\tau \gtrsim 0.1$, the constitutive equations (2.7) no longer hold, our nonlinear fit

analysis seems to indicate that the dampening coefficients α_d and α_λ plateau at large τ . This conclusion is not necessarily meaningful, since the ansatz (2.20) that the time dependence of δn , δP and β is of the form $e^{-\alpha t}$ with constant α is not guaranteed to be valid in the transition regime. It is certain that the time dependence of the above quantities is more complex at large values of τ , since the dissipative exponential attenuation is replaced by a polynomial dispersive attenuation in the ballistic regime, as will be shown in Sec. VI.

G. Summary

In this section, we analysed the attenuation of a longitudinal wave using the equations of first-order hydrodynamics. The results obtained by numerically solving the AWB equation at small values of the relaxation time τ showed an excellent agreement with the analytic results when the transport coefficients λ and η were obtained using the Chapman-Enskog method. The analytic results corresponding to the transport coefficients obtained using the Grad method exhibited a clear discrepancy compared to the numerical results.

We further tested the validity of the linearised form of the AWB equation (2.18) by comparing the numerical and analytic results at increasing values of the wave amplitudes, while keeping $\tau = 0.0083$. A visible discrepancy can be seen at wave amplitudes of $\beta_0, \delta n_0/n_0, \delta P_0/P_0 \gtrsim 0.1$. We also considered the applicability of the functional form of the solution of the first order hydrodynamics equations by numerically fitting the attenuation coefficients α_λ and α_η , as well as the oscillation frequency α_o , to the numerical results. Our analysis shows that the best fit parameters differ significantly from the analytic prediction when the wave amplitude is $\gtrsim 0.1$. At smaller values of the wave amplitudes, the numerical results clearly favoured the Chapman-Enskog predictions for the transport coefficients, while the Grad predictions showed a visible discrepancy to the numerical results.

Finally, we considered the validity of the first-order hydrodynamics equations at increasing values of τ . We found that the dampening coefficients α_d and α_λ are directly proportional to τ only for $\tau \lesssim 0.1$, being in excellent agreement with the Chapman-Enskog prediction. At larger values of τ , they increase at a much slower rate, signaling the breakdown of the hydrodynamics formulation when $\tau \gtrsim 0.1$. The Grad prediction was in clear disagreement with the numerical results for all values of τ .

IV. SECOND ORDER HYDRODYNAMICS

The five-field theory provides the constitutive equations for q^μ and $\Pi^{\mu\nu}$ in the form given in Eq. (3.1). Since these constitutive equations do not represent evolution equations, q^μ and $\Pi^{\mu\nu}$ are fully determined by the spatial and temporal gradients of n , u^μ and P . In particular, their initial values at $t = 0$ cannot be set to arbitrary values. In this section, we will employ the second order extension of the five-field theory in order to study the relaxation process of the heat flux and shear stress from their initial vanishing value to the value required through the constitutive equations of the five-field theory.

A. Constitutive relations

There are many variations of the form in which the equations of the second order hydrodynamics (also known as extended irreversible thermodynamics [32]) are presented, essentially due to the route adopted in deriving them [10, 33–37]. In this section, we will consider the form introduced in Refs. [32, 33], according to which q^μ and $T^{\mu\nu}$ satisfy the following equations:

$$\begin{aligned} q^\mu &= -\lambda T \Delta^{\mu\nu} \left[\partial_\nu \ln T + u^\rho \partial_\rho u_\nu + \beta_1 u^\rho \partial_\rho q_\nu - \alpha_1 \partial_\rho \Pi^\rho_\nu \right. \\ &\quad \left. - (1 - \gamma_1) T \Pi^\rho_\nu \partial_\rho \left(\frac{\alpha_1}{T} \right) + \frac{1}{2} T q_\nu \partial_\rho \left(\frac{\beta_1 u^\rho}{T} \right) \right], \\ \Pi^{\mu\nu} &= -\eta \left(\Delta^{\mu\lambda} \Delta^{\nu\kappa} + \Delta^{\nu\lambda} \Delta^{\mu\kappa} - \frac{2}{3} \Delta^{\mu\nu} \Delta^{\lambda\kappa} \right) \\ &\quad \times \left[\partial_\lambda u_\kappa + \beta_2 u^\rho \partial_\rho \Pi_{\lambda\kappa} - \alpha_1 \partial_\lambda q_\kappa - \gamma_1 T q_\lambda \partial_\kappa \left(\frac{\alpha_1}{T} \right) + \frac{1}{2} T \Pi_{\lambda\kappa} \partial_\rho \left(\frac{\beta_2 u^\rho}{T} \right) \right], \end{aligned} \quad (4.1)$$

where the thermodynamic coefficients β_1 , β_2 and γ_1 and the viscous-heat flux coupling coefficient α_1 are *a priori* not known. After performing the linearisation described in Sec. II B, Eq. (4.1) becomes:

$$\tau_q \partial_t q + q = -\frac{\lambda P_0}{4n_0} \left(\frac{3\partial_z \delta P}{P_0} - \frac{4\partial_z \delta n}{n_0} \right) + \frac{\lambda}{4n_0} (1 + 4\alpha_1 P_0) \partial_z \Pi, \quad (4.2a)$$

$$\tau_\Pi \partial_t \Pi + \Pi = -\frac{4\eta}{3} \partial_z (\beta - \alpha_1 q), \quad (4.2b)$$

where Eq. (2.22c) was used to eliminate the time derivative of β in Eq. (4.2a), while the relaxation times were defined as $\tau_q = \lambda(T\beta_1 - 1/4n_0)$ and $\tau_\Pi = 2\eta\beta_2$. In order for the

constitutive equation for q and Π to match the first-order versions (3.4) in the limit $\tau_q, \tau_\Pi \rightarrow 0$, we set $\alpha_1 = -1/4P_0$ and Eqs. (4.2) reduce to:

$$\tau_q \partial_t q + q = -\frac{\lambda P_0}{4n_0} \left(\frac{3\partial_z \delta P}{P_0} - \frac{4\partial_z \delta n}{n_0} \right), \quad (4.3a)$$

$$\tau_\Pi \partial_t \Pi + \Pi = -\frac{4\eta}{3} \partial_z \left(\beta + \frac{q}{4P_0} \right), \quad (4.3b)$$

By analogy to Eq. (3.2), we introduce the reduced relaxation times $\tau_{q,0}$ and $\tau_{\Pi,0}$ through:

$$\tau_q = \tau_{q,0} \tau, \quad \tau_\Pi = \tau_{\Pi,0} \tau. \quad (4.4)$$

In general, the values of $\tau_{q,0}$ and $\tau_{\Pi,0}$ are determined by the properties of the collision term in the Boltzmann equation. When the Anderson-Witting single relaxation time approximation is used, the following values for $\tau_{q,0}$ and $\tau_{\Pi,0}$ are commonly employed within both the Chapman-Enskog- and moment-like methods [14, 28, 37, 40, 41]:

$$\tau_{\Pi,0} = 1, \quad \tau_{q,0} = 1. \quad (4.5)$$

It is interesting to test the hyperbolicity of the resulting set of equations. Equations (2.17) and (4.3) can be written in the following form:

$$\partial_t \mathbb{U} + \partial_z (\mathbb{A} \mathbb{U}) = \mathbb{S}, \quad (4.6)$$

where

$$\begin{aligned} \mathbb{U} &= \left(\frac{\delta n}{n_0}, \frac{\delta P}{P_0}, \beta, \frac{q}{P_0}, \frac{\Pi}{P_0} \right)^T, \\ \mathbb{S} &= \left(0, 0, \frac{q}{4\tau_q P_0}, -\frac{q}{\tau_q P_0}, -\frac{\Pi}{\tau_\Pi P_0} \right)^T, \end{aligned} \quad (4.7)$$

while \mathbb{A} is given by:

$$\mathbb{A} = \begin{pmatrix} 0 & 0 & 1 & 0 & 0 \\ 0 & 0 & \frac{4}{3} & \frac{1}{3} & 0 \\ \frac{\lambda_0}{4\tau_{q,0}} & \frac{1}{4} - \frac{3\lambda_0}{16\tau_{q,0}} & 0 & 0 & \frac{1}{4} \\ -\frac{\lambda_0}{\tau_{q,0}} & \frac{3\lambda_0}{4\tau_{q,0}} & 0 & 0 & 0 \\ 0 & 0 & \frac{4\eta_0}{3\tau_{\Pi,0}} & \frac{\eta_0}{3\tau_{\Pi,0}} & 0 \end{pmatrix}. \quad (4.8)$$

The eigenvalues of \mathbb{A} can be found analytically and are given by:

$$a_0 = 0, \quad a_{\lambda,\pm} = \pm \frac{1}{2} \sqrt{\frac{\lambda_0}{\tau_{q,0}}}, \quad a_{\eta,\pm} = \pm \frac{1}{\sqrt{3}} \sqrt{1 + \frac{\eta_0}{\tau_{\Pi,0}}}. \quad (4.9)$$

Since the eigenvalues of \mathbb{A} are real, the system of equations (4.6) is hyperbolic [32, 42].

B. Longitudinal waves: modes

Employing the ansatz (A1) allows Π_α to be expressed from Eq. (4.3b) as follows:

$$\Pi_\alpha = -\frac{4k\eta}{3(1-\alpha\tau_\Pi)} \left(\beta_\alpha + \frac{q_\alpha}{4P_0} \right). \quad (4.10)$$

Furthermore, Eq. (2.22b) allows δP_α to be written as:

$$\delta P_\alpha = \frac{4P_0k}{3\alpha} \left(\beta_\alpha + \frac{q_\alpha}{4P_0} \right). \quad (4.11)$$

Inserting Eq. (4.10) and (4.11) into Eq. (2.22c) yields:

$$\left[\alpha + \frac{k^2}{3\alpha} - \frac{\eta k^2}{3P_0(1-\alpha\tau_\Pi)} \right] \left(\beta_\alpha + \frac{q_\alpha}{4P_0} \right) = 0. \quad (4.12)$$

The above equation is satisfied when either of the two factors cancel. We shall treat these two cases separately in what follows.

a. $q_\alpha = -4P_0\beta_\alpha$. This case is also recovered for q_λ in the first-order approximation (3.9). In this case, Eqs. (4.10) and (4.11) show that $\Pi_\alpha = \delta P_\alpha = 0$. The values of α corresponding to this regime can be found from Eq. (4.3a), which reduces to:

$$\left[\frac{\lambda k^2}{\alpha n_0} - 4(1-\alpha\tau_q) \right] \beta_\alpha = 0. \quad (4.13)$$

The case $\beta_\alpha = 0$ trivially corresponds to a vanishing perturbation (i.e. $\delta n_\alpha = \delta P_\alpha = 0$). Setting the term inside the square bracket to 0 yields the following values for α :

$$\begin{aligned} \alpha_{\lambda,+} &= \frac{1}{2\tau_q} \left(1 + \sqrt{1 - \frac{k^2\lambda\tau_q}{n_0}} \right) \simeq \frac{1}{\tau_q} - \alpha_\lambda + O(\tau^3), \\ \alpha_{\lambda,-} &= \frac{1}{2\tau_q} \left(1 - \sqrt{1 - \frac{k^2\lambda\tau_q}{n_0}} \right) \simeq \alpha_\lambda + O(\tau^3). \end{aligned} \quad (4.14)$$

It can be seen that, in the small τ limit, $\alpha_{\lambda,-}$ corresponds to the dampening coefficient $\alpha_\lambda = k^2\lambda/4n_0$ identified in the first order theory (3.8). The term $\alpha_{\lambda,+}$ allows \tilde{q} to relax from an arbitrary initial condition at $t = 0$ to the first-order expression (3.4) on a timescale of order τ_q . The modes corresponding to the above values of $\alpha_{\lambda,\pm}$ can be written in terms of the amplitudes $\beta_{\lambda,\pm}$ as follows:

$$\delta n_{\lambda,\pm} = \frac{kn_0}{\alpha_{\lambda,\pm}} \beta_{\lambda,\pm}, \quad q_{\lambda,\pm} = -4P_0\beta_{\lambda,\pm}, \quad \delta P_{\lambda,\pm} = \Pi_{\lambda,\pm} = 0. \quad (4.15)$$

The square root in the definition of $\alpha_{\lambda,\pm}$ (4.14) becomes imaginary when $\tau > \tau_{\lambda,\text{lim}}$, where

$$\tau_{\lambda,\text{lim}} = \frac{1}{k\sqrt{\tau_{q,0}\lambda_0}}. \quad (4.16)$$

When $0 < \tau < \tau_{\lambda,\text{lim}}$, the modes corresponding to $\alpha_{\lambda,\pm}$ are overdamped (evanescent), while when $\tau > \tau_{\lambda,\text{lim}}$, the underdamped regime settles in. In order to treat both regimes within a unitary framework, it is convenient to cast Eq. (4.14) in the form $\alpha_{\lambda,\pm} = \alpha_{\lambda,d} \pm \alpha_{\lambda,o} = \alpha_{\lambda,d} \pm i\bar{\alpha}_{\lambda,o}$, where we have introduced:

$$\alpha_{\lambda,d} = \frac{1}{2\tau_q}, \quad \alpha_{\lambda,o} = \alpha_{\lambda,d} \sqrt{1 - \frac{k^2 \lambda \tau_q}{n_0}}, \quad \bar{\alpha}_{\lambda,o} = \alpha_{\lambda,d} \sqrt{\frac{k^2 \lambda \tau_q}{n_0} - 1}. \quad (4.17)$$

b. $q_\alpha = 0$. We now consider the case when the first bracket in Eq. (4.12) vanishes. It can be seen that $q_\alpha = 0$ in this case by using Eqs. (2.22a), (4.10) and (4.11) in Eq. (4.3a).

The allowed values for α can be found by solving the following cubic equation:

$$\left(\frac{3\alpha^2}{k^2} + 1 \right) (1 - \alpha\tau_\Pi) - \frac{\eta\alpha}{P_0} = 0. \quad (4.18)$$

Equation (4.18) has the roots $\alpha \in \{\alpha_{\eta,r}, \alpha_{\eta,\pm}\}$, where we set $\alpha_{\eta,\pm} = \alpha_{\eta,d} \pm i\alpha_{\eta,o}$ by analogy to the first order case (3.11). The exact expressions for the coefficients $\alpha_{\eta,r}$, $\alpha_{\eta,d}$ and $\alpha_{\eta,o}$ are:

$$\begin{aligned} \alpha_{\eta,r} &= \frac{1}{3\tau_\Pi} \left\{ 1 + \frac{1}{R_\eta} \left[1 - k^2 \tau_\Pi^2 \left(1 + \frac{\eta}{\tau_\Pi P_0} \right) \right] + R_\eta \right\} \simeq \frac{1}{\tau_\Pi} - 2\alpha_d + O(\tau^3), \\ \alpha_{\eta,d} &= \frac{1}{3\tau_\Pi} \left\{ 1 - \frac{1}{2R_\eta} \left[1 - k^2 \tau_\Pi^2 \left(1 + \frac{\eta}{\tau_\Pi P_0} \right) \right] - \frac{R_\eta}{2} \right\} \simeq \alpha_d + O(\tau^3), \\ \alpha_{\eta,o} &= \frac{\sqrt{3}}{6\tau_\Pi} \left\{ \frac{1}{R_\eta} \left[1 - k^2 \tau_\Pi^2 \left(1 + \frac{\eta}{\tau_\Pi P_0} \right) \right] - R_\eta \right\} \simeq \alpha_o + O(\tau^2), \end{aligned} \quad (4.19)$$

where

$$R_\eta = \begin{cases} \left[1 - 3k\tau_\Pi \sqrt{R_{\eta,\text{aux}}} + 3k^2 \tau_\Pi^2 \left(1 - \frac{\eta}{2P_0 \tau_\Pi} \right) \right]^{1/3}, & 0 < \tau < \tau_{\eta,\text{lim}}, \\ - \left[-1 + 3k\tau_\Pi \sqrt{R_{\eta,\text{aux}}} - 3k^2 \tau_\Pi^2 \left(1 - \frac{\eta}{2P_0 \tau_\Pi} \right) \right]^{1/3}, & \tau > \tau_{\eta,\text{lim}}. \end{cases} \quad (4.20)$$

In the above, we have introduced:

$$R_{\eta,\text{aux}} = 1 + \frac{2}{3} k^2 \tau_\Pi^2 \left(1 - \frac{5\eta}{2P_0 \tau_\Pi} - \frac{\eta^2}{8P_0^2 \tau_\Pi^2} \right) + \frac{k^4 \tau_\Pi^4}{9} \left(1 + \frac{\eta}{P_0 \tau_\Pi} \right)^3. \quad (4.21)$$

The parameter $\tau_{\eta,\text{lim}}$ is defined as the value of τ at which the expression under the cubic root in Eq. (4.20) vanishes. It is given by:

$$\tau_{\eta,\text{lim}} = \frac{1}{k\tau_{\Pi,0} \sqrt{1 + \eta_0/\tau_{\Pi,0}}}. \quad (4.22)$$

The definition (4.20) of R_η ensures that the coefficients $\alpha_{\eta,*}$ ($* \in \{r, d, o\}$), defined in Eq. (4.19), are real for all positive values of τ , provided that $R_{\eta,\text{aux}} > 0$. In order to investigate the latter inequality, it is convenient to consider $\eta/\tau_\Pi P_0$ as an independent parameter. In this case, the roots of $R_{\eta,\text{aux}}$ are:

$$(k^2 \tau_\Pi^2)_\pm = \frac{3(\eta/\tau_\Pi P_0)^2 + 20(\eta/\tau_\Pi P_0) - 8 \pm [(\eta/\tau_\Pi P_0) - 8]^{3/2}}{8 - 1 + 3(\eta/\tau_\Pi P_0) + 3(\eta/\tau_\Pi P_0)^2 + (\eta/\tau_\Pi P_0)^2}. \quad (4.23)$$

It can be seen that $(k^2 \tau_\Pi^2)_\pm$ is real only when $\eta/\tau_\Pi P_0 \geq 8$. In the hydrodynamic regime, the Chapman-Enskog expansion (3.3b) together with Eq. (4.5) predict that $\eta/\tau_\Pi P_0 = 4/5$, which is much smaller than 8. For the sake of simplicity, we will not consider the case when $(k^2 \tau_\Pi^2)_\pm$ are real. Instead, we shall consider that the coefficients $\alpha_{\eta,*}$ (4.19) are real for all values of τ considered in this section. It is worth mentioning that setting $\eta_0 = 4/5$, $\tau_{\Pi,0} = 1$ and $k = 2\pi$ in Eq. (4.22) yields $\tau_{\eta,\text{lim}} \simeq 0.12$, which is within the range of values of τ considered in Subsec. IV D.

The small τ expansion of Eq. (4.19) reveals the first order coefficients $\alpha_d = k^2 \eta / 6 P_0$ and $\alpha_o = k / \sqrt{3} + O(\tau^2)$ reported in Eq. (3.12). The coefficient $\alpha_{\eta,r}$ was not present in the first order theory and in this case it corresponds to the mode that ensures the relaxation of $\tilde{\Pi}$ from $\tilde{\Pi}(t=0) = 0$ to the value predicted through the constitutive equation of the first order theory.

C. Longitudinal waves: solution

The full solution of the longitudinal wave problem can be written in general in the following form:

$$\widetilde{M} = \widetilde{M}_\lambda + \widetilde{M}_\eta, \quad (4.24)$$

where $\widetilde{M} \in \{\widetilde{\beta}, \widetilde{\delta n}, \widetilde{\delta P}, \widetilde{q}, \widetilde{\Pi}\}$. The subscripts λ and η refer to the parts of the solution corresponding to $\alpha_{\lambda,\pm}$ and $\alpha_{\eta,*}$ ($* \in \{r, d, o\}$), respectively.

According to Eq. (4.15), $\widetilde{\delta P}_\lambda = \widetilde{\Pi}_\lambda = 0$, while $\widetilde{\beta}_\lambda$, $\widetilde{\delta n}_\lambda$ and \widetilde{q}_λ can be written for $\tau < \tau_{\lambda,\text{lim}}$ (4.16) as:

$$\begin{pmatrix} \widetilde{\beta}_\lambda \\ \widetilde{\delta n}_\lambda \\ \widetilde{q}_\lambda \end{pmatrix}_{\tau < \tau_{\lambda,\text{lim}}} = e^{-\alpha_{\lambda,d} t} \left[\begin{pmatrix} \beta_{\lambda,c} \\ \delta n_{\lambda,c} \\ q_{\lambda,c} \end{pmatrix} \cosh \alpha_{\lambda,o} t + \begin{pmatrix} \beta_{\lambda,s} \\ \delta n_{\lambda,s} \\ q_{\lambda,s} \end{pmatrix} \sinh \alpha_{\lambda,o} t \right]. \quad (4.25)$$

When $\tau > \tau_{\lambda, \text{lim}}$, the hyperbolic functions in the above expression become trigonometric functions:

$$\begin{pmatrix} \widetilde{\beta}_\lambda \\ \widetilde{\delta n}_\lambda \\ \widetilde{q}_\lambda \end{pmatrix}_{\tau_q > \tau_{q, \text{lim}}} = e^{-\bar{\alpha}_{\lambda, d} t} \left[\begin{pmatrix} \bar{\beta}_{\lambda, c} \\ \bar{\delta n}_{\lambda, c} \\ \bar{q}_{\lambda, c} \end{pmatrix} \cos \bar{\alpha}_{\lambda, o} + \begin{pmatrix} \bar{\beta}_{\lambda, s} \\ \bar{\delta n}_{\lambda, s} \\ \bar{q}_{\lambda, s} \end{pmatrix} \sin \bar{\alpha}_{\lambda, o} \right]. \quad (4.26)$$

The constants $\beta_{\lambda, *}$ and $\bar{\beta}_{\lambda, *}$ (where $* \in \{c, s\}$) are fixed by the initial conditions, while:

$$\begin{aligned} q_{\lambda, *} &= -4P_0 \beta_{\lambda, *}, & \bar{q}_{\lambda, *} &= -4P_0 \bar{\beta}_{\lambda, *}, \\ \delta n_{\lambda, c} &= kn_0 \frac{\alpha_{\lambda, d} \beta_{\lambda, c} + \alpha_{\lambda, o} \beta_{\lambda, s}}{\alpha_{\lambda, d}^2 - \alpha_{\lambda, o}^2}, & \bar{\delta n}_{\lambda, c} &= kn_0 \frac{\bar{\alpha}_{\lambda, d} \bar{\beta}_{\lambda, c} + \bar{\alpha}_{\lambda, o} \bar{\beta}_{\lambda, s}}{\bar{\alpha}_{\lambda, d}^2 + \bar{\alpha}_{\lambda, o}^2}, \\ \delta n_{\lambda, s} &= kn_0 \frac{\alpha_{\lambda, d} \beta_{\lambda, s} + \alpha_{\lambda, o} \beta_{\lambda, c}}{\alpha_{\lambda, d}^2 - \alpha_{\lambda, o}^2}, & \bar{\delta n}_{\lambda, s} &= kn_0 \frac{\bar{\alpha}_{\lambda, d} \bar{\beta}_{\lambda, s} - \bar{\alpha}_{\lambda, o} \bar{\beta}_{\lambda, c}}{\bar{\alpha}_{\lambda, d}^2 + \bar{\alpha}_{\lambda, o}^2}. \end{aligned} \quad (4.27)$$

The part of the solution (4.24) corresponding to $\alpha_{\eta, *}$ ($* \in \{r, d, o\}$) can be written as:

$$\begin{pmatrix} \widetilde{\beta}_\eta \\ \widetilde{\delta n}_\eta \\ \widetilde{\delta P}_\eta \\ \widetilde{\Pi}_\eta \end{pmatrix} = \begin{pmatrix} \beta_{\eta, r} \\ \delta n_{\eta, r} \\ \delta P_{\eta, r} \\ \Pi_{\eta, r} \end{pmatrix} e^{-\alpha_{\eta, r}} + \left[\begin{pmatrix} \beta_{\eta, c} \\ \delta n_{\eta, c} \\ \delta P_{\eta, c} \\ \Pi_{\eta, c} \end{pmatrix} \cos \alpha_{\eta, o} + \begin{pmatrix} \beta_{\eta, s} \\ \delta n_{\eta, s} \\ \delta P_{\eta, s} \\ \Pi_{\eta, s} \end{pmatrix} \sin \alpha_{\eta, o} \right] e^{-\alpha_{\eta, d}}, \quad (4.28)$$

while $\widetilde{q}_\eta = 0$. The integration constants $\beta_{\eta, *}$ are fixed by the initial conditions, while

$$\begin{aligned} \begin{pmatrix} \delta n_{\eta, r} \\ \delta P_{\eta, r} \\ \Pi_{\eta, r} \end{pmatrix} &= \begin{pmatrix} kn_0 / \alpha_{\eta, r} \\ 4P_0 k / 3 \alpha_{\eta, r} \\ -4k\eta / 3 (1 - \alpha_{\eta, r} \tau_\Pi) \end{pmatrix} \beta_{\eta, r}, \\ \begin{pmatrix} \delta n_{\eta, c} \\ \delta P_{\eta, c} \end{pmatrix} &= \begin{pmatrix} kn_0 \\ 4P_0 k / 3 \end{pmatrix} \frac{\alpha_{\eta, d} \beta_{\eta, c} + \alpha_{\eta, o} \beta_{\eta, s}}{\alpha_{\eta, d}^2 + \alpha_{\eta, o}^2}, \\ \begin{pmatrix} \delta n_{\eta, s} \\ \delta P_{\eta, s} \end{pmatrix} &= \begin{pmatrix} kn_0 \\ 4P_0 k / 3 \end{pmatrix} \frac{\alpha_{\eta, d} \beta_{\eta, s} - \alpha_{\eta, o} \beta_{\eta, c}}{\alpha_{\eta, d}^2 + \alpha_{\eta, o}^2}, \\ \Pi_{\eta, c} &= -\frac{4k\eta}{3} \frac{(1 - \alpha_{\eta, d} \tau_\Pi) \beta_{\eta, c} - \alpha_{\eta, o} \tau_\Pi \beta_{\eta, s}}{(1 - \alpha_{\eta, d} \tau_\Pi)^2 + (\alpha_{\eta, o} \tau_\Pi)^2}, \\ \Pi_{\eta, s} &= -\frac{4k\eta}{3} \frac{(1 - \alpha_{\eta, d} \tau_\Pi) \beta_{\eta, s} + \alpha_{\eta, d} \tau_\Pi \beta_{\eta, c}}{(1 - \alpha_{\eta, d} \tau_\Pi)^2 + (\alpha_{\eta, o} \tau_\Pi)^2}. \end{aligned} \quad (4.29)$$

The initial conditions (2.23) for $\widetilde{\beta}$, $\widetilde{\delta n}$ and $\widetilde{\delta P}$ are supplemented by

$$\widetilde{q}(t=0) = 0, \quad \widetilde{\Pi}(t=0) = 0. \quad (4.30)$$

Substituting the solution (4.24) into the initial conditions equations (2.23) and (4.30) yields:

$$\begin{aligned}\beta_{\lambda,c} + \beta_{\eta,r} + \beta_{\eta,c} &= \beta_0, & \delta n_{\lambda,c} + \delta n_{\eta,r} + \delta n_{\eta,c} &= \delta n_0, \\ \delta P_{\eta,r} + \delta P_{\eta,c} &= \delta P_0, & q_{\lambda,c} &= 0, & \delta \Pi_{\eta,r} + \delta \Pi_{\eta,c} &= 0.\end{aligned}\quad (4.31)$$

The equation $q_{\lambda,c} = 0$ implies that $\beta_{\lambda,c} = 0$ (this is also true when $\tau_q > \tau_{q,\text{lim}}$, i.e. $\bar{q}_{\lambda,c} = \bar{\beta}_{\lambda,c} = 0$). Furthermore, noting that $\delta P_{\eta,*} = 4P_0\delta n_{\eta,*}/3n_0$, the second equality in Eq. (4.31) implies:

$$\left(\frac{\beta_{\lambda,s}}{\bar{\beta}_{\lambda,s}}\right) = \frac{1}{4k} \left(\frac{(\alpha_{\lambda,d}^2 - \alpha_{\lambda,o}^2)/\alpha_{\lambda,o}}{(\bar{\alpha}_{\lambda,d}^2 + \bar{\alpha}_{\lambda,o}^2)/\bar{\alpha}_{\lambda,o}} \right) \left(\frac{4\delta n_0}{n_0} - \frac{3\delta P_0}{P_0} \right). \quad (4.32a)$$

Next, $\beta_{\eta,r}$ and $\beta_{\eta,s}$ can be written as:

$$\begin{aligned}\beta_{\eta,r} &= -\frac{\alpha_{\eta,r}(1 - \alpha_{\eta,r}\tau_{\Pi})}{\tau_{\Pi}[\alpha_{\eta,o}^2 + (\alpha_{\eta,d} - \alpha_{\eta,r})^2]} \left[\beta_0 - \frac{3\tau_{\Pi}\delta P_0}{4kP_0}(\alpha_{\eta,d}^2 + \alpha_{\eta,o}^2) \right], \\ \beta_{\eta,s} &= \frac{\alpha_{\eta,d}^2 + \alpha_{\eta,o}^2}{4k\alpha_{\eta,o}} \frac{3\delta P_0}{P_0} - \frac{\alpha_{\eta,d}}{\alpha_{\eta,o}} \beta_0 - \frac{\alpha_{\eta,d}^2 + \alpha_{\eta,o}^2 - \alpha_{\eta,d}\alpha_{\eta,r}}{\alpha_{\eta,r}\alpha_{\eta,o}} \beta_{\eta,r},\end{aligned}\quad (4.32b)$$

while $\beta_{\eta,c} = \beta_0 - \beta_{\eta,r}$.

We will now consider the above analytic results to study the relaxation process for \tilde{q} and $\tilde{\Pi}$ in the context of *Case 1* and *Case 2b* introduced in Sec. II C.

D. Case 1: Adiabatic flow

Setting $\delta n_0 = \delta P_0 = 0$ in Eq. (4.32a) yields $\beta_{\lambda,s} = 0$, such that $\widetilde{M}_{\lambda} = 0$ for all $\widetilde{M} \in \{\widetilde{\beta}, \widetilde{\delta n}, \widetilde{\delta P}, \widetilde{q}, \widetilde{\Pi}\}$. The integration constants $\beta_{\eta,r}$, $\beta_{\eta,c}$ and $\beta_{\eta,s}$ can be found from Eq. (4.32b) as follows:

$$\begin{aligned}\beta_{\eta,r} &= -\frac{\alpha_{\eta,r}(1 - \alpha_{\eta,r}\tau_{\Pi})}{\tau_{\Pi}[\alpha_{\eta,o}^2 + (\alpha_{\eta,d} - \alpha_{\eta,r})^2]} \beta_0, \\ \beta_{\eta,c} &= \beta_0 \left[1 + \frac{\alpha_{\eta,r}(1 - \alpha_{\eta,r}\tau_{\Pi})}{\tau_{\Pi}[\alpha_{\eta,o}^2 + (\alpha_{\eta,d} - \alpha_{\eta,r})^2]} \right], \\ \beta_{\eta,s} &= \frac{\beta_0}{\alpha_{\eta,o}\tau_{\Pi}} \frac{(\alpha_{\eta,d}^2 + \alpha_{\eta,o}^2 - \alpha_{\eta,d}\alpha_{\eta,r})(1 - \alpha_{\eta,d}\tau_{\Pi}) - \alpha_{\eta,r}\alpha_{\eta,o}^2\tau_{\Pi}}{\alpha_{\eta,o}^2 + (\alpha_{\eta,d} - \alpha_{\eta,r})^2}.\end{aligned}\quad (4.33)$$

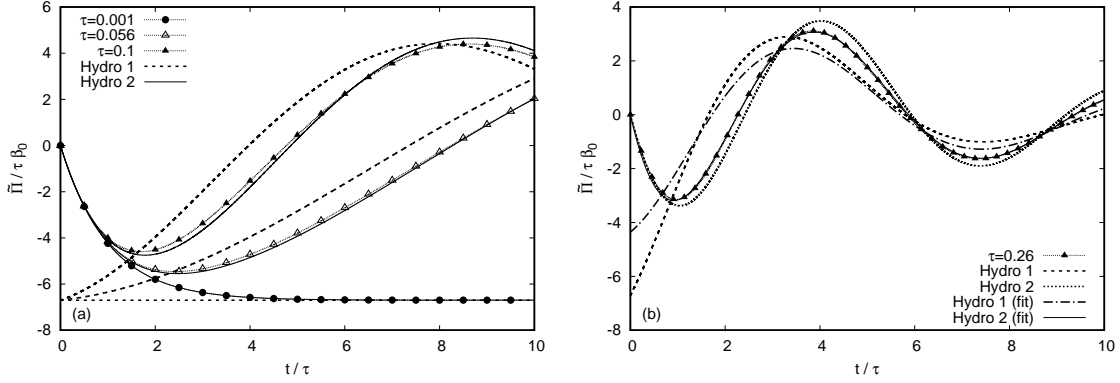


FIG. 6. (a) Numerical results (dotted lines and points) for the evolution of $\tilde{\Pi}/\tau\beta_0$ at various values of τ for $\beta_0 = 10^{-3}$ (to ease the comparison, the horizontal axis shows t/τ). The analytic curves corresponding to the first (3.20) and second (4.34) order hydrodynamics are shown using dotted and continuous lines, respectively. (b) Time evolution of $\tilde{\Pi}/\tau\beta_0$ at $\tau = 0.26$ and $\beta_0 = 10^{-3}$. The fitted curve corresponding to the first order hydrodynamics is obtained by performing a nonlinear fit of Eq. (3.20) using α_η and α_o as free parameters. In the second order case, the nonlinear fit is performed on Eq. (4.34) by considering $\alpha_{\eta,r}$, $\alpha_{\eta,d}$, $\alpha_{\eta,o}$ and the ratio η/τ_Π as free parameters. All non-fitted analytic curves are obtained using the Chapman-Enskog value for η_0 (3.3b) and $\tau_{\Pi,0} = 1$ (4.5).

Substituting the above expressions in Eq. (4.29) yields:

$$\begin{aligned}
 \begin{pmatrix} \delta n_{\eta,r} \\ \delta P_{\eta,r} \\ \Pi_{\eta,r} \end{pmatrix} &= - \begin{pmatrix} \delta n_{\eta,c} \\ \delta P_{\eta,c} \\ \Pi_{\eta,c} \end{pmatrix} = \begin{pmatrix} -kn_0(1 - \alpha_{\eta,r}\tau_\Pi) \\ -4kP_0(1 - \alpha_{\eta,r}\tau_\Pi)/3 \\ 4k\eta\alpha_{\eta,r}/3 \end{pmatrix} \frac{\beta_0}{\tau_\Pi[\alpha_{\eta,o}^2 + (\alpha_{\eta,d} - \alpha_{\eta,r})^2]}, \\
 \begin{pmatrix} \delta n_{\eta,s} \\ \delta P_{\eta,s} \end{pmatrix} &= \begin{pmatrix} \delta n_{\eta,r} \\ \delta P_{\eta,r} \end{pmatrix} \frac{\alpha_{\eta,d} - \alpha_{\eta,r} - (\alpha_{\eta,d}^2 + \alpha_{\eta,o}^2 - \alpha_{\eta,d}\alpha_{\eta,r})\tau_\Pi}{\alpha_{\eta,o}(1 - \alpha_{\eta,r}\tau_\Pi)}, \\
 \Pi_{\eta,s} &= -\Pi_{\eta,r} \frac{\alpha_{\eta,d}^2 + \alpha_{\eta,o}^2 - \alpha_{\eta,d}\alpha_{\eta,r}}{\alpha_{\eta,o}\alpha_{\eta,r}}.
 \end{aligned} \tag{4.34}$$

The validity of the solution (4.34) is inspected in Fig. 6(a). At small values of τ , $\tilde{\Pi}$ relaxes from its initial vanishing value to the value predicted by the first order expression (3.20) after a time $t \sim 5\tau$. For $\tau \gtrsim 0.05$, the first order approximation becomes non-satisfactory at small values of t , since it lags behind the numerical solution. At small τ , the second order approximation is overlapped with the numerical solution for all values of t . A discrepancy

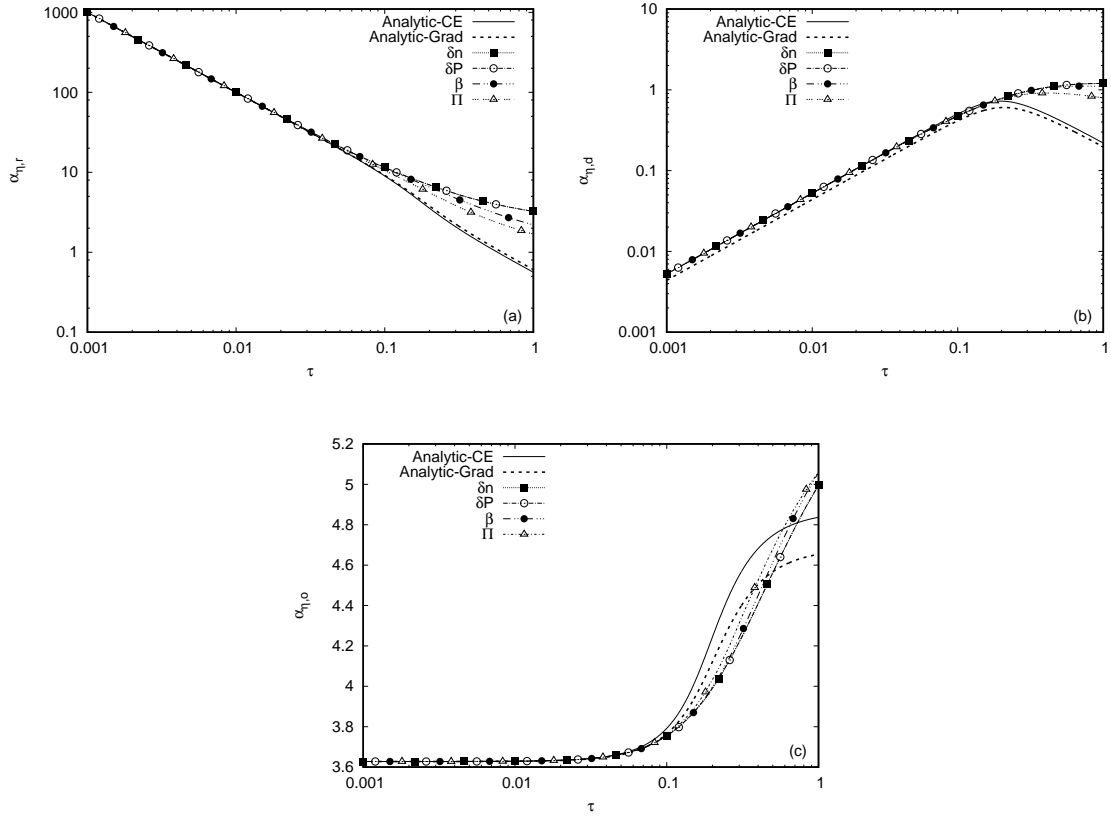


FIG. 7. Comparison with respect to τ between the analytic prediction (4.19) and the numerical fit for the coefficients (a) $\alpha_{\eta,r}$, (b) $\alpha_{\eta,d}$ and (c) $\alpha_{\eta,o}$. The analytic curves corresponding to the Chapman-Enskog procedure (continuous lines) and Grad moment method (dotted lines) are obtained by using the expressions (3.3b) and (3.3a) for η_0 in Eq. (4.19). The numerical curves (dotted lines and points) are obtained by performing a nonlinear fit on the functional forms (4.28) of $\tilde{\beta}$, $\tilde{\delta n}$, $\tilde{\delta P}$ and $\tilde{\Pi}$. The simulations were initialised according to *Case 1*, i.e. $\delta n_0 = \delta P_0 = 0$ and $\beta_0 = 10^{-3}$.

between the second order prediction and the numerical result can be seen when $\tau \gtrsim 0.05$. As shown in Fig. 6(b), at small enough values for τ , this discrepancy arises when the values of η_0 and $\tau_{\Pi,0}$ predicted by Eqs. (3.3b) and (4.5) are used in the analytic expression. If instead, these values are treated as free parameters, the functional form (4.34) can be used to accurately represent $\tilde{\Pi}$, even at $\tau \simeq 0.26$.

We now test the validity of Eqs. (3.3b) and (4.5) pertaining to the Chapman-Enskog expressions for η_0 and $\tau_{\Pi,0}$. For this purpose, we will perform a nonlinear fit of the functional

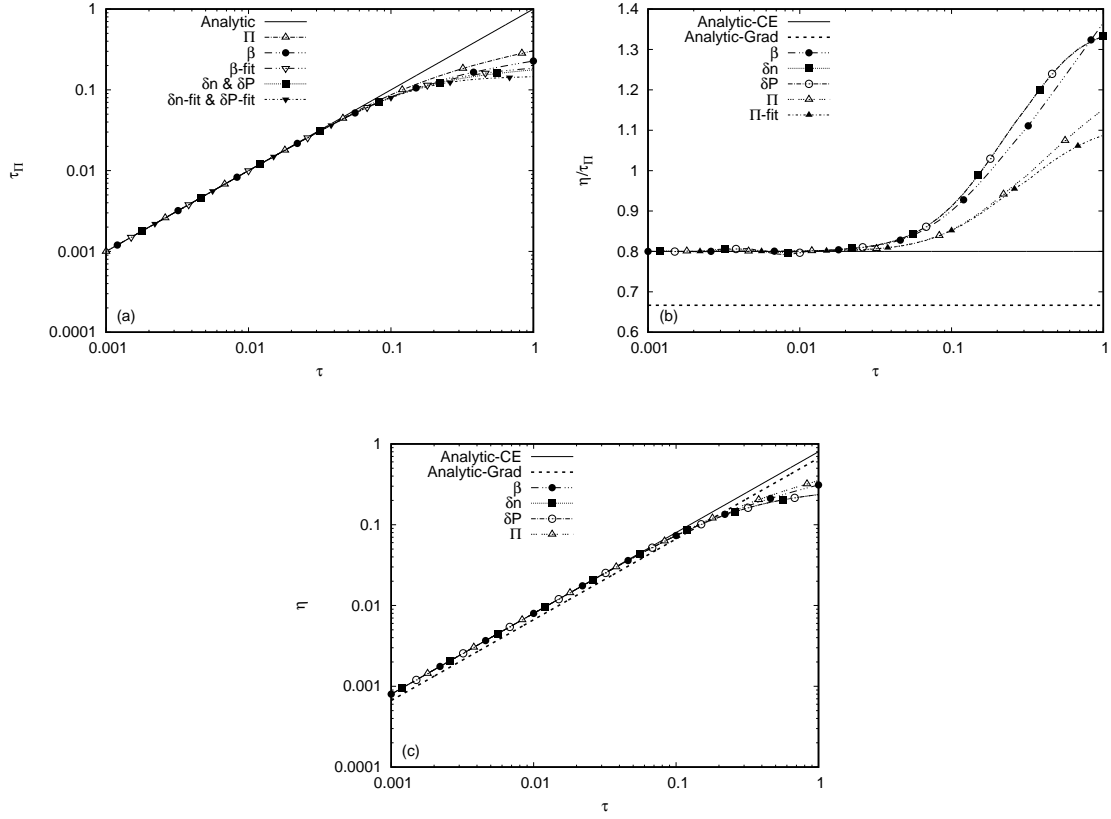


FIG. 8. Comparison with respect to τ between the analytic and numerical predictions for (a) the relaxation time τ_{Π} ; (b) the ratio $\eta/\tau_{\Pi}P_0$; (c) the coefficient of shear viscosity η . The analytic expression for τ_{Π} (continuous line), given in Eq. (4.5), is $\tau_{\Pi} = \tau$, while the analytic expression for $\eta/\tau_{\Pi}P_0 = \eta_0$ is given in Eqs. (3.3b) and (3.3a) for the Chapman-Enskog (continuous line) and Grad (dotted lines) cases. The numerical results (dotted lines and points) are obtained as described in Sec. IVD.

forms in Eq. (4.34), where the coefficients $\alpha_{\eta,r}$, $\alpha_{\eta,d}$ and $\alpha_{\eta,o}$ are considered free parameters. In addition, the solutions for $\widetilde{\delta n}$ and $\widetilde{\delta P}$ depend explicitly on τ_{Π} , while $\widetilde{\Pi}$ depends explicitly on η/τ_{Π} . The inversion of Eq. (4.19) would allow η and τ_{Π} to be written in terms of $\alpha_{\eta,r}$ and $\alpha_{\eta,d}$, but this operation is mathematically intractable. We will thus also treat τ_{Π} as a free parameter for $\widetilde{\delta n}$ and $\widetilde{\delta P}$, while in the case of $\widetilde{\Pi}$, we will consider η/τ_{Π} as an independent parameter. The results of the numerical fits for $\alpha_{\eta,r}$, $\alpha_{\eta,d}$ and $\alpha_{\eta,o}$ are presented in Fig. 7. In the case of the $\alpha_{\eta,r}$ coefficient, it can be seen that the analytic expression predicts a sharper decrease at large τ compared to the numerical results. The shapes of $\alpha_{\eta,d}$ and

$\alpha_{\eta,o}$ remain qualitatively similar to those obtained for α_d and α_o in the first order theory, which are shown in Fig. 5. In the first order theory, α_d is directly proportional to τ , while the numerical results seem to indicate a saturation of α_d for $\tau \gtrsim 0.1$. This saturation can be seen also for $\alpha_{\eta,d}$, but in this case, the analytic expression predicts that $\alpha_{\eta,d}$ decreases with τ . Another notable difference can be seen in the analytic prediction for $\alpha_{\eta,o}$, which in the second order case qualitatively follows the numerical results ($\alpha_{\eta,o}$ increases at large τ) compared to the first order case, when α_o is predicted to decrease at large τ .

We end this section by performing an analysis of the dependence of the relaxation time τ_{Π} and of the ratio $\eta/\tau_{\Pi}P_0$ on τ . The curves shown in Fig. 8 represent three types of results. First, the analytic predictions for τ_{Π} (4.5) is shown in Fig. 8(a) using a continuous line, while the Chapman-Enskog and Grad predictions for $\eta/P_0\tau_{\Pi}$ are shown in Fig. 8(b) using continuous and dotted lines. Second, the results of the nonlinear fit procedure described in the previous paragraph for τ_{Π} (obtained from $\widetilde{\beta}$, $\widetilde{\delta n}$ and $\widetilde{\delta P}$) and for $\eta/\tau_{\Pi}P_0$ (obtained from $\widetilde{\Pi}$) are labelled using the suffix “-fit”. The rest of the curves are obtained by numerically finding the values of τ_{Π} and $\eta/\tau_{\Pi}P_0$ for which the roots of Eq. (4.18) correspond to the values of $\alpha_{\eta,r}$ and $\alpha_{\eta,d}$ obtained through the nonlinear fit procedure (the value of $\alpha_{\eta,o}$ is not taken into account in this algorithm). As expected, the relaxation time τ_{Π} stops increasing linearly with τ when $\tau \gtrsim 0.1$. Figure 8(b) shows that the ratio $\eta/\tau_{\Pi}P_0$ increases with τ , which seems to indicate that the increase of the shear viscosity of the gas with respect to τ is of higher order than the linear prediction of the first order theory (3.1). However, Fig. 8(c) shows that in fact η (obtained by multiplying the results for $\eta/\tau_{\Pi}P_0$ and τ_{Π} obtained as explained above) increases at a sub-linear rate with respect to τ when $\tau \gtrsim 0.1$. This result is consistent with that obtained in Fig. 5 in the first order case. When $\tau \lesssim 0.1$, our numerical results favour the Chapman-Enskog prediction for the transport coefficients, as well as the relations (4.5).

E. Non-adiabatic flow

Let us now focus on *Case 2b*, when $\beta_0 = \delta P_0 = 0$. This case is particularly simple since, according to Eq. (4.32b), $\beta_{\eta,*} = 0$ for all $\eta \in \{r, c, s\}$. The only non-vanishing integration constants are $\beta_{\lambda,s}$ (overdamped case) and $\overline{\beta}_{\lambda,s}$ (underdamped case), which can be found from

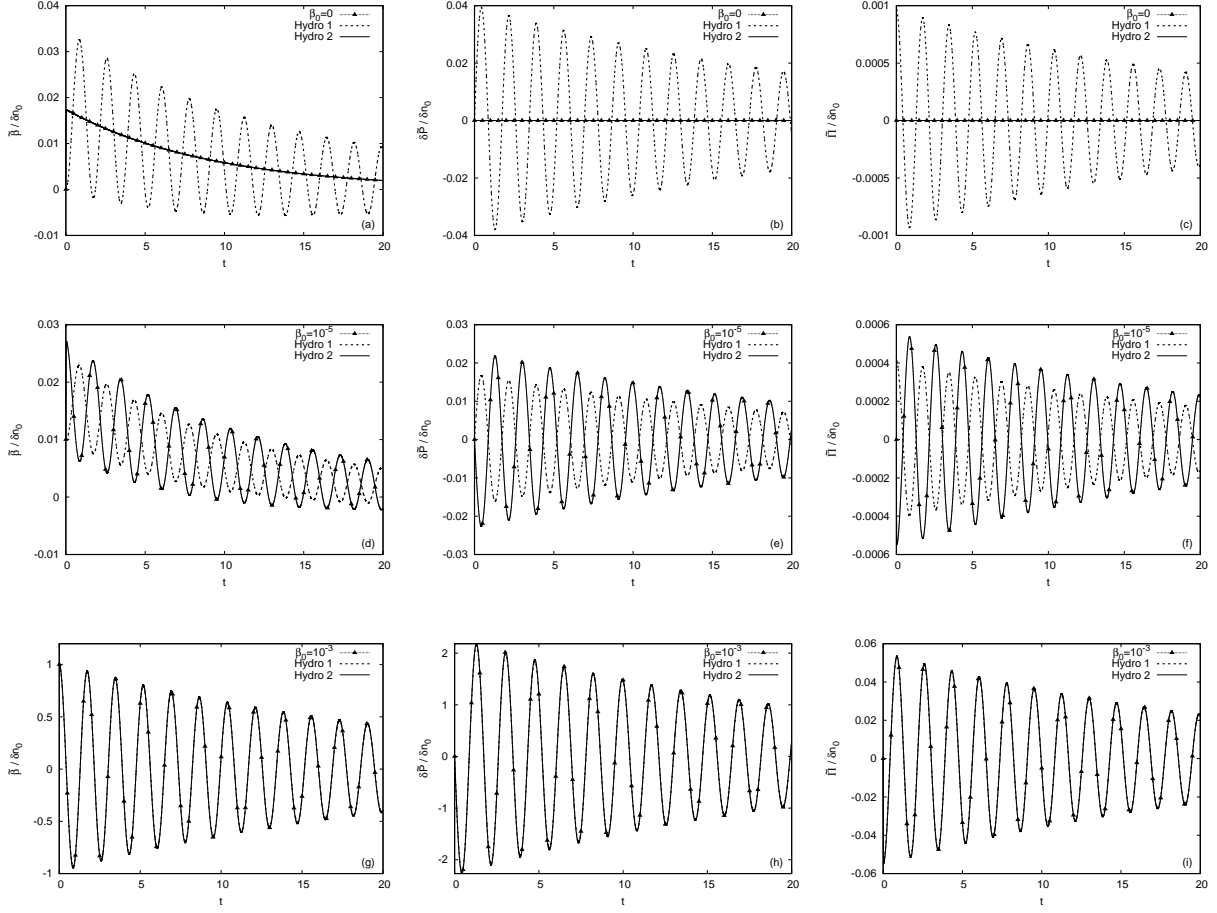


FIG. 9. Comparison between the numerical results (dotted lines and points) for $\tilde{\beta}$ (first column), $\tilde{\delta P}$ (second column) and $\tilde{\Pi}$ (third column) and the corresponding analytic predictions of the first order (dotted lines) and second order (continuous lines) hydrodynamics when $\tau_{\Pi} = \tau$ and the Chapman-Enskog value (3.3b) for η is employed. The initial conditions for the plots on the first line correspond to *Case 2b*, i.e. $\beta_0 = \delta P_0 = 0$ and $\delta n_0 = 10^{-3}$. On the second line, β_0 is increased to 10^{-5} and on the third line, $\beta_0 = 10^{-3}$. All curves are normalised with respect to $\delta n_0 = 10^{-3}$ and $\tau = 0.0083$ was used throughout the simulations.

Eq. (4.32a):

$$\left(\frac{\beta_{\lambda,s}}{\bar{\beta}_{\lambda,s}} \right) = \left(\frac{(\alpha_{\lambda,d}^2 - \alpha_{\lambda,o}^2)/\alpha_{\lambda,o}}{(\bar{\alpha}_{\lambda,d}^2 + \bar{\alpha}_{\lambda,o}^2)/\bar{\alpha}_{\lambda,o}} \right) \frac{\delta n_0}{k n_0}. \quad (4.35)$$

Noting that $\widetilde{\delta P} = \widetilde{\Pi} = 0$ by virtue of Eq. (4.28), the full solution in the overdamped case reads:

$$\begin{aligned}\widetilde{\beta} &= \frac{\delta n_0}{kn_0} \frac{\alpha_{\lambda,d}^2 - \alpha_{\lambda,o}^2}{\alpha_{\lambda,o}} e^{-\alpha_{\lambda,d}t} \sinh \alpha_{\lambda,o}t, \\ \widetilde{\delta n} &= \delta n_0 \left(\cosh \alpha_{\lambda,o}t + \frac{\alpha_{\lambda,d}}{\alpha_{\lambda,o}} \sinh \alpha_{\lambda,o}t \right) e^{-\alpha_{\lambda,d}t}, \\ \widetilde{q} &= -4P_0 \frac{\delta n_0}{kn_0} \frac{\alpha_{\lambda,d}^2 - \alpha_{\lambda,o}^2}{\alpha_{\lambda,o}} e^{-\alpha_{\lambda,d}t} \sinh \alpha_{\lambda,o}t,\end{aligned}\tag{4.36a}$$

while in the underdamped case, the solution reads:

$$\begin{aligned}\widetilde{\beta} &= \frac{\delta n_0}{kn_0} \frac{\overline{\alpha}_{\lambda,d}^2 + \overline{\alpha}_{\lambda,o}^2}{\overline{\alpha}_{\lambda,o}} e^{-\overline{\alpha}_{\lambda,d}t} \sin \overline{\alpha}_{\lambda,o}t, \\ \widetilde{\delta n} &= \delta n_0 \left(\cos \overline{\alpha}_{\lambda,o}t + \frac{\overline{\alpha}_{\lambda,d}}{\overline{\alpha}_{\lambda,o}} \sin \overline{\alpha}_{\lambda,o}t \right) e^{-\overline{\alpha}_{\lambda,d}t}, \\ \widetilde{q} &= -4P_0 \frac{\delta n_0}{kn_0} \frac{\overline{\alpha}_{\lambda,d}^2 + \overline{\alpha}_{\lambda,o}^2}{\overline{\alpha}_{\lambda,o}} e^{-\overline{\alpha}_{\lambda,d}t} \sin \overline{\alpha}_{\lambda,o}t.\end{aligned}\tag{4.36b}$$

In the first order theory, Eq. (3.17) predicts that, when $\beta_0 = \delta P_0 = 0$, β_c and β_s become proportional to δn_0 , which also implies that $\widetilde{\Pi}$ and $\widetilde{\delta P}$ are non-zero. This discrepancy between the first order and second order theories holds for any value of τ , hence it cannot be considered a “higher order” effect. Instead, it represents a fundamental flaw of the first order theory. This case is represented in the plots on the first line of Fig. 9, where the time evolution of $\widetilde{\beta}$, $\widetilde{\delta P}$ and $\widetilde{\Pi}$ (normalised with respect to δn_0) is represented for the initial conditions $\delta n_0 = 10^{-3}$, $\delta P_0 = 0$ and $\beta_0 = 0$. Both the second order theory and the numerical results indicate that $\widetilde{\delta P}$ and $\widetilde{\Pi}$ remain zero throughout the evolution, while the first order result predicts oscillations of these quantities. Moreover, in the first order theory, $\widetilde{\beta}$ presents strong oscillations about a decaying exponential, which are not present when the second order theory is employed.

The discussion in the preceding paragraph suggests that the first order theory cannot fully recover the hydrodynamic regime (small τ) of the decaying longitudinal wave when the initialisation is performed according to *Case 2b*, i.e. $\beta_0 = \delta P_0 = 0$ and $\delta n_0 = 10^{-3}$. We further test if this conclusion holds at non-vanishing values of β_0 . The second and third lines of Fig. 9 show the evolution of $\widetilde{\beta}$, $\widetilde{\delta P}$ and $\widetilde{\Pi}$ (again normalised with respect to δn_0) when $\beta_0 = 10^{-5}$ and $\beta_0 = 10^{-3}$, respectively. At $\beta_0 = 10^{-5}$, the first order theory predicts oscillations which are (nearly) in antiphase to the numerical and second order theory results.

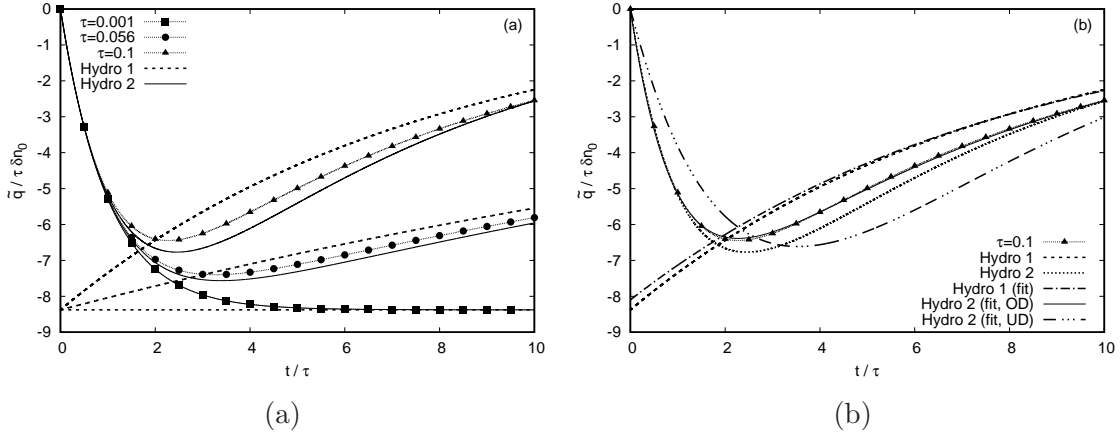


FIG. 10. (a) Numerical results (dotted lines and points) for the evolution of $\tilde{q}/\tau\delta n_0$ at various values of τ for $\delta n_0 = 10^{-3}$ (to ease the comparison, the horizontal axis shows t/τ). The analytic curves corresponding to the first (3.20) and second (4.34) order hydrodynamics are shown using dotted and continuous lines, respectively. (b) Time evolution of $\tilde{q}/\tau\delta n_0$ at $\tau = 0.1$ and $\delta n_0 = 10^{-3}$. The fitted curve corresponding to the first order hydrodynamics is obtained by performing a nonlinear fit of Eq. (3.21) using α_η and α_o as free parameters. In the second order case, the nonlinear fit is performed on Eqs. (4.36a) and (4.36b) for the overdamped and underdamped cases by considering $\alpha_{\lambda,d}$ and $\alpha_{\eta,o}$ ($\bar{\alpha}_{\lambda,d}$ and $\bar{\alpha}_{\lambda,o}$) as free parameters. All non-fitted analytic curves are obtained using the Chapman-Enskog value for λ_0 (3.3b) and $\tau_{q,0} = 1$ (4.5).

When $\beta_0 = 10^{-3}$, the discrepancy between the curves corresponding to the first order theory and the numerical and second order theory results is no longer visible.

The ability of the second order hydrodynamics to capture the relaxation of \tilde{q} from 0 at initial time to the value predicted by the first order theory is investigated in Fig. 10(a). It can be seen that at small τ , \tilde{q} relaxes to the value predicted through the first order theory after a time $t \sim 5\tau$. At $\tau \gtrsim 0.1$, the first order approximation seems to no longer agree with the numerical solution, while the second order approximation slowly loses its validity. In Fig. 10(b), the numerical result for the evolution of \tilde{q} at $\tau = 0.1$ is compared to the first (3.21) and second (4.36a) order hydrodynamics predictions, specialised to the Chapman-Enskog case, when $\lambda_0 = 4/3$ and $\tau_{q,0} = 1$. It can be seen that there is significant discrepancy between the analytic and numerical results. The curve labelled *Hydro 1 (fit)* represents the best fit to the numerical results of the functional form of the analytic solution (3.21),

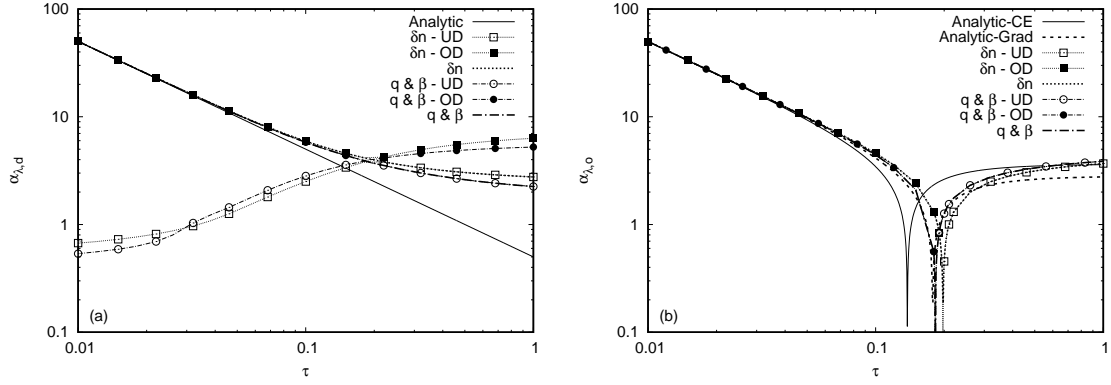


FIG. 11. Analysis with respect to τ of (a) $\alpha_{\lambda,d}$ and (b) $\alpha_{\lambda,o}$ for the initial conditions of *Case 2b* (i.e. $\beta_0 = \delta P_0 = 0$ and $\delta n_0 = 10^{-3}$). The analytic curve in (a) is $\alpha_{\lambda,d} = 1/2\tau$, while in (b), the analytic result (4.17) is represented using the Chapman-Enskog (continuous line) and Grad (dashed line) values for λ , while τ_q was taken equal to τ . The numerical curves shown with dotted lines and filled symbols are obtained by performing a nonlinear fit on the overdamped (OD) solution (4.36a) while considering $\alpha_{\lambda,d}$ and $\alpha_{\lambda,o}$ as free parameters. The dotted lines and hollow symbols are obtained by fitting the values of $\bar{\alpha}_{\lambda,d}$ and $\bar{\alpha}_{\lambda,o}$ to the numerical results using the underdamped solution (4.36b). The numerical curves represented with dashed lines and without points are obtained by combining the UD results ($\tau \lesssim 0.2$) with the OD results ($\tau \gtrsim 0.2$). The transition from the OD to the UD regime occurs when $\alpha_{\lambda,o} = 0$, as indicated by the spikes in (b).

with α_λ considered as a free parameter. The second order fits are performed on the two functional forms (4.36a) and (4.36b), corresponding to the overdamped and underdamped cases, respectively. In the overdamped case, Eq. (4.36a) is fitted to the numerical data by considering $\alpha_{\lambda,d}$ and $\alpha_{\lambda,o}$ as free parameters. In the underdamped case, $\bar{\alpha}_{\lambda,d}$ and $\bar{\alpha}_{\lambda,o}$ are found by performing a nonlinear fit of Eq. (4.36b) with respect to the numerical data. It can be seen in Fig. 10(b) that, at $\tau = 0.1$, the first order and second order underdamped fits still present significant deviations from the numerical curve. However, the second order overdamped fit is in very good agreement with the numerical result, validating the functional form (4.36a) for $\tau \lesssim 0.1$.

Next, Fig. 11 shows an analysis of $(\alpha_{\lambda,d}, \alpha_{\lambda,o})$ and $(\bar{\alpha}_{\lambda,d}, \bar{\alpha}_{\lambda,o})$ as obtained by performing a two-parameter nonlinear fit of Eqs. (4.36a) and (4.36b) for the overdamped (OD) and underdamped (UD) regimes, respectively, to the numerical results obtained for $\tilde{\beta}$, $\tilde{\delta n}$ and

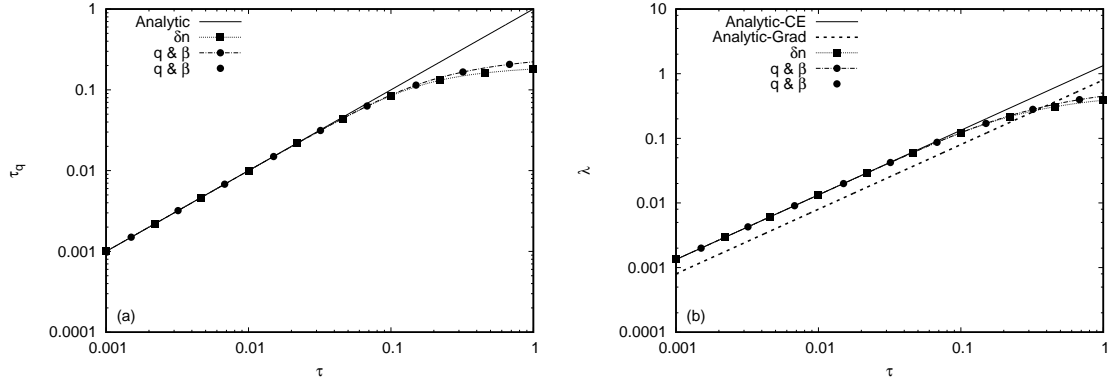


FIG. 12. Analysis with respect to τ of (a) τ_q and (b) λ for the initial conditions of *Case 2b* (i.e. $\beta_0 = \delta P_0 = 0$ and $\delta n_0 = 10^{-3}$). The analytic curve shown in (a) using a continuous line is $\tau_q = \tau$, while in (b), the analytic curves correspond to the Chapman-Enskog (continuous line) and Grad (dotted line) values for λ , given in Eqs. (3.3b) and (3.3a), respectively. The numerical results are obtained as explained in Sec. IV E.

\tilde{q} . Only the initialisation corresponding to *Case 2b* (i.e. $\beta_0 = \delta P_0 = 0$ and $\delta n_0 = 10^{-3}$) is considered here. The numerical fit confirms that at small values of τ , $\alpha_{\lambda,d}$ and $\alpha_{\lambda,o} \simeq 1/2\tau$. Furthermore, the results shown in Fig. 11(a) for α_λ indicate that the UD regime is not valid when $\tau \lesssim 0.2$, while the OD regime loses applicability when $\tau \gtrsim 0.2$. This can also be seen in Fig. 11(b), where the strong spikes indicate the points where $\alpha_{\lambda,o} = 0$, i.e. where the transition from the UD to the OD regime occurs. According to Eq. (5.27), this happens when $\tau = \tau_{\lambda,\text{lim}}^{\text{CE}} \simeq 0.138$ and $\tau = \tau_{\lambda,\text{lim}}^{\text{G}} \simeq 0.1779$ when the Chapman-Enskog (3.3b) and Grad (3.3a) values for λ_0 are used, respectively. Our numerical analysis indicates that $\tau_{\lambda,\text{lim}} \simeq 0.199$ (in the case of $\tilde{\delta n}$) and $\tau_{\lambda,\text{lim}} \simeq 0.183$ (in the case of $\tilde{\beta}$ and \tilde{q}), higher than both the Chapman-Enskog and the Grad predictions.

We now turn to the analysis of the relaxation time τ_q and the heat conductivity λ , shown in Fig. 12. In order to extract the values of these coefficients from our numerical results, we start from the numerical fits of $\alpha_{\lambda,d}$ and $\alpha_{\lambda,o}$, where the overdamped (OD) and underdamped (UD) values are taken when $\tau < \tau_{q,\text{lim}}$ and $\tau > \tau_{q,\text{lim}}$, respectively. Next, we seek the values of λ and τ_q such that the roots $\alpha_{\lambda,\pm}$ (4.14) satisfy:

$$\frac{\alpha_{\lambda,+} + \alpha_{\lambda,-}}{2} = \alpha_{\lambda,d}, \quad \left| \frac{\alpha_{\lambda,+} - \alpha_{\lambda,-}}{2} \right| = \alpha_{\lambda,o}, \quad (4.37)$$

where the absolute value is interpreted in the usual sense in the case when $\alpha_{\lambda,\pm}$ are complex

numbers. The results for τ_q and λ are shown in Figs. 12(a) and 12(b), respectively. It can be seen that the numerical results for τ_q agree with the theoretical prediction $\tau_q = \tau$ at small values of τ , while for larger values of τ , τ_q seems to reach a plateau. The curve representing the numerical results for λ is practically overlapped with the Chapman-Enskog prediction (3.3b), while at larger values of τ , λ seems to reach a plateau, in good qualitative agreement with the predictions of the first order theory presented in Fig. 5.

F. Summary

In this section, we employed a particular form of the second order hydrodynamics equations to study the attenuation of a longitudinal wave in the linearised regime. More precisely, we chose a coupling constant $\alpha_1 = -1/4P_0$ between the shear pressure Π and heat flux q in the theory presented in Refs. [32, 33], in order to ensure consistency with the first order hydrodynamics analysis presented in Sec. III.

The main aim of this section is to confirm that the second order hydrodynamics correctly describes the relaxation process of Π and q from essentially arbitrary initial values (both vanish at initial time in our analysis) to some non-zero value which agrees with the prediction of the first-order theory at small enough values of τ . This is shown in Figs. 6 and 10, while the values of the relaxation times τ_Π and τ_q are analysed with respect to the relaxation time τ of the Anderson-Witting model in Figs. 8 and 12.

During our analysis, we have pointed out a fundamental inconsistency of the first order theory, which we summarise as follows. If at initial time, the velocity and pressure perturbations vanish (i.e. $\beta_0 = \delta P_0 = 0$), the pressure $\widetilde{\delta P}$ and shear stress $\widetilde{\Pi}$ perturbations remain zero at all later times, while the attenuation of $\widetilde{\beta}$ is purely evanescent (non-oscillatory). This result is obtained analytically in the second order theory and is confirmed via numerical simulations in Fig. 9. On the other hand, the first order theory predicts that $\widetilde{\delta P}$ and $\widetilde{\Pi}$ are proportional to δn_0 and $\widetilde{\beta}$ has an oscillatory component whose amplitude is proportional to τ . We are thus led to the conclusion that the first order theory cannot correctly describe this particular dissipative process, even when the relaxation time is small.

V. MOMENT METHOD

The analysis presented in the previous sections provides indication that the correct expression for the transport coefficients λ and η is obtained using the Chapman-Enskog procedure. Recently [28], it was shown that one of the main drawbacks of the moment method as originally employed by Israel and Stewart [10] is that the distribution function f is expanded with respect to the nonorthogonal basis formed of powers of p^μ . Truncating this series at a finite order discards an infinite number of terms of first order with respect to the Knudsen number Kn ($\text{Kn} \sim \tau$). The solution proposed in Ref. [28] was to expand f with respect to irreducible tensors with respect to the particle momentum p^μ . The proposed scheme recovers the expressions for the transport coefficients λ and η obtained using the Chapman-Enskog expansion.

In this section, we consider a moment-based method similar to the one introduced in Ref. [28]. We employ spherical coordinates $\{p, \theta, \varphi\}$ in the momentum space and expand the distribution function f with respect to the generalised Laguerre polynomials for the momentum magnitude p , the Legendre polynomials for $\xi = \cos \theta$ and the trigonometric basis $\{\cos m\varphi, \sin m\varphi\}$ for φ . Due to the symmetries of the system, f can be considered independent of φ , such that only the p and ξ expansions will be discussed. Truncating the system at order $N_L = 1$ and $N_\xi = 2$ yields a system of six equations for the five hydrodynamical variables δn , β , δP , q and Π , as well as a non-hydrodynamic (ghost) variable. We illustrate the importance of this sixth variable in establishing the symmetry between the shear stress and heat flux solutions, such that the underdamped (UD) and overdamped (OD) regimes discussed in Sec. IV are represented unitarily in this new solution.

A. Constitutive relations

In this section, we again approach the longitudinal wave problem, but this time by employing a moment method. Instead of performing the standard Grad-like expansion of f in terms of polynomials in p^μ , we follow Refs. [20, 21] and expand f as follows:

$$f = \frac{1}{T_0^3} e^{-p/T_0} \sum_{\ell=0}^{\infty} \frac{1}{(\ell+1)(\ell+2)} \mathcal{F}_\ell L_\ell^{(2)}(p/T_0), \quad (5.1)$$

where $L_\ell^{(2)}(z)$ are the generalised Laguerre polynomial of type 2 and order ℓ , which satisfy the following orthogonality relation:

$$\int_0^\infty dz z^2 e^{-z} L_\ell^{(2)}(z) L_{\ell'}^{(2)}(z) = (\ell+1)(\ell+2) \delta_{\ell,\ell'}. \quad (5.2)$$

Thus, the coefficients \mathcal{F}_ℓ can be obtained as follows:

$$\mathcal{F}_\ell = \int_0^\infty dp p^2 f L_\ell^{(2)}(p/T_0). \quad (5.3)$$

Multiplying the Boltzmann equation (2.18), valid only in the linearised regime of the longitudinal wave problem, by $p^2 L_\ell^{(2)}(p/T_0)$ and integrating over p yields:

$$\partial_t \mathcal{F}_\ell + \xi \partial_z \mathcal{F}_\ell = -\frac{1}{\tau} (\mathcal{F}_\ell - \mathcal{F}_\ell^{(\text{eq})}), \quad (5.4)$$

where the coefficients $\mathcal{F}_\ell^{(\text{eq})}$ corresponding to the equilibrium distribution function $f^{(\text{eq})}$ are defined by analogy to Eq. (5.3):

$$\mathcal{F}_\ell^{(\text{eq})} = \int_0^\infty dp p^2 f^{(\text{eq})} L_\ell^{(2)}(p/T_0). \quad (5.5)$$

In the absence of collisions [i.e. when neglecting the right hand side in Eq. (5.4)], each coefficient \mathcal{F}_ℓ evolves independently. Since $f^{(\text{eq})}$ is constructed only in terms of N^μ and $T^{\mu\nu}$, which correspond to $\ell = 0$ and $\ell = 1$, the evolution of N^μ and $T^{\mu\nu}$ is fully determined by considering Eq. (5.4) only for $\ell = 0$ and $\ell = 1$ and neglecting all higher ℓ terms [20].

We further expand \mathcal{F}_ℓ with respect to ξ using the complete set of Legendre polynomials $P_\ell(\xi)$:

$$\mathcal{F}_\ell = \sum_{s=0}^\infty \frac{2s+1}{2} \mathcal{F}_{\ell,s} P_s(\xi), \quad (5.6)$$

where the coefficients $\mathcal{F}_{\ell,s}$ depend only on z and t and are obtained using the orthogonality of the Legendre polynomials as follows:

$$\mathcal{F}_{\ell,s} = \int_{-1}^1 d\xi \mathcal{F}_\ell P_s(\xi). \quad (5.7)$$

The coefficients $\mathcal{F}_{\ell,s}^{(\text{eq})}$ corresponding to $f^{(\text{eq})}$ can be defined in a similar manner:

$$\mathcal{F}_{\ell,s}^{(\text{eq})} = \int_{-1}^1 d\xi \mathcal{F}_\ell^{(\text{eq})} P_s(\xi). \quad (5.8)$$

The expansion coefficients $\mathcal{F}_{\ell,s}$ can be linked to N^μ and $T^{\mu\nu}$ as follows:

$$\begin{aligned} \mathcal{F}_{0,0} &= N^t = n_0 + \delta n, & \mathcal{F}_{0,1} &= N^z \simeq n_0 \beta, & \mathcal{F}_{1,0} &= 3N^t - \frac{1}{T_0} T^{tt} \simeq 3n_0 \left(\frac{\delta n}{n_0} - \frac{\delta P}{P_0} \right), \\ \mathcal{F}_{1,1} &= 3N^z - \frac{1}{T_0} T^{tz} \simeq -n_0 \beta - \frac{q}{T_0}, & 3\mathcal{F}_{0,2} - \mathcal{F}_{1,2} &\simeq \frac{\Pi}{T_0}. \end{aligned} \quad (5.9)$$

The coefficients $\mathcal{F}_{0,2}$ and $\mathcal{F}_{1,2}$ on their own have no correspondent with respect to N^μ and $T^{\mu\nu}$. The equilibrium coefficients $\mathcal{F}_{\ell,s}^{(\text{eq})}$ ($\ell = 0, 1$ and $s = 0, 1, 2$) can be found from Eq. (2.19):

$$\begin{aligned}\mathcal{F}_{0,0}^{(\text{eq})} &\simeq n_0 + \delta n, & \mathcal{F}_{0,1}^{(\text{eq})} &\simeq n_0\beta + \frac{q}{4T_0}, & \mathcal{F}_{0,2}^{(\text{eq})} &\simeq 0, \\ \mathcal{F}_{1,0}^{(\text{eq})} &\simeq 3n_0 \left(\frac{\delta n}{n_0} - \frac{\delta P}{P_0} \right), & \mathcal{F}_{1,1}^{(\text{eq})} &\simeq -n_0\beta - \frac{q}{4T_0}, & \mathcal{F}_{1,2}^{(\text{eq})} &\simeq 0.\end{aligned}\quad (5.10)$$

Using the recurrence relation:

$$\xi P_s(\xi) = \frac{s+1}{2s+1} P_{s+1}(\xi) + \frac{s}{2s+1} P_{s-1}(\xi), \quad (5.11)$$

Eq. (5.5) can be projected on the space of the Legendre polynomials as follows:

$$\partial_t \mathcal{F}_{\ell,s} + \partial_z \left(\frac{s+1}{2s+1} \mathcal{F}_{\ell,s+1} + \frac{s}{2s+1} \mathcal{F}_{\ell,s-1} \right) = -\frac{1}{\tau} (\mathcal{F}_{\ell,s} - \mathcal{F}_{\ell,s}^{(\text{eq})}). \quad (5.12)$$

The above procedure produces an infinite system of equations corresponding to various values of (ℓ, s) , where knowledge of $\mathcal{F}_{\ell,s+1}$ is required in order to determine the evolution of $\mathcal{F}_{\ell,s}$. As also discussed in Ref. [20], the above system can be closed at an order Q by imposing $\mathcal{F}_{\ell,Q} = 0$. This procedure is intimately related to the numerical method employed in this paper (described in detail in Ref. [20] and also summarised in Appendix A). In particular, Q represents the quadrature order of the model and the resulting system of equations is guaranteed to be hyperbolic. Since in this section we are only interested in the study of N^μ and $T^{\mu\nu}$, we will henceforth consider only the case $Q = 3$, such that $\mathcal{F}_{0,3} = \mathcal{F}_{1,3} = 0$. The resulting set of equations can be written as:

$$\partial_t \mathcal{F}_{0,0} + \partial_z \mathcal{F}_{0,1} = -\frac{1}{\tau} (\mathcal{F}_{0,0} - \mathcal{F}_{0,0}^{(\text{eq})}), \quad (5.13a)$$

$$\partial_t \mathcal{F}_{0,1} + \partial_z \left(\frac{1}{3} \mathcal{F}_{0,0} + \frac{2}{3} \mathcal{F}_{0,2} \right) = -\frac{1}{\tau} (\mathcal{F}_{0,1} - \mathcal{F}_{0,1}^{(\text{eq})}), \quad (5.13b)$$

$$\partial_t \mathcal{F}_{0,2} + \frac{2}{5} \partial_z \mathcal{F}_{0,1} = -\frac{1}{\tau} \mathcal{F}_{0,2}, \quad (5.13c)$$

$$\partial_t \mathcal{F}_{1,0} + \partial_z \mathcal{F}_{1,1} = -\frac{1}{\tau} (\mathcal{F}_{1,0} - \mathcal{F}_{1,0}^{(\text{eq})}), \quad (5.13d)$$

$$\partial_t \mathcal{F}_{1,1} + \partial_z \left(\frac{1}{3} \mathcal{F}_{1,0} + \frac{2}{3} \mathcal{F}_{1,2} \right) = -\frac{1}{\tau} (\mathcal{F}_{1,1} - \mathcal{F}_{1,1}^{(\text{eq})}), \quad (5.13e)$$

$$\partial_t \mathcal{F}_{0,2} + \frac{2}{5} \partial_z \mathcal{F}_{0,1} = -\frac{1}{\tau} \mathcal{F}_{0,2}. \quad (5.13f)$$

The above system is closed. Substituting Eqs. (5.9) and (5.10) into Eq. (5.13), the conservation equations (2.17) can be obtained, together with the following constitutive equations:

$$\tau \partial_t q + q = -\frac{\tau P_0}{3} \partial_z \left(\frac{3\delta P}{P_0} - \frac{4\delta n}{n_0} \right) + \frac{2P_0\tau}{3n_0} \partial_z (\mathcal{F}_{0,2} + \mathcal{F}_{1,2}), \quad (5.14a)$$

$$\tau \partial_t \Pi + \Pi = -\frac{16\tau P_0}{15} \partial_z \left(\beta + \frac{q}{4P_0} \right), \quad (5.14b)$$

$$(\tau \partial_t + 1)(\mathcal{F}_{0,2} + \mathcal{F}_{1,2}) = \frac{2n_0\tau}{5P_0} \partial_z q. \quad (5.14c)$$

Comparing the above equations to the second-order hydrodynamics constitutive equations (4.3), it can be seen that the transport coefficients have the following expressions:

$$\lambda = \frac{4}{3}\tau n_0, \quad \eta = \frac{4}{5}\tau P_0, \quad \tau_q = \tau, \quad \tau_\Pi = \tau. \quad (5.15)$$

The above relations confirm the Chapman-Enskog prediction (3.3b) for λ and η and agree with the second-order hydrodynamics (4.5) values for τ_q and τ_Π . Furthermore, the constitutive equation (5.14a) contains an extra term compared to the second-order hydrodynamics version (4.3a). A simple power counting shows that this term is cubic in the relaxation time τ , hence it cannot be present in the second-order hydrodynamics theory.

B. Longitudinal waves: modes

Let us now apply the ansatz (2.20) to the new variables $\mathcal{F}_{0,2}$ and $\mathcal{F}_{1,2}$:

$$\mathcal{F}_{0,2} = \tilde{\mathcal{F}}_{0,2} \cos kz, \quad \mathcal{F}_{1,2} = \tilde{\mathcal{F}}_{1,2} \cos kz. \quad (5.16)$$

The mode decomposition (2.21) can be applied to $\tilde{\mathcal{F}}_{0,2}$ and $\tilde{\mathcal{F}}_{1,2}$ as follows:

$$\begin{pmatrix} \tilde{\mathcal{F}}_{0,2} \\ \tilde{\mathcal{F}}_{1,2} \end{pmatrix} = \sum_{\alpha} \begin{pmatrix} \mathcal{F}_{0,2;\alpha} \\ \mathcal{F}_{1,2;\alpha} \end{pmatrix} e^{-\alpha t}. \quad (5.17)$$

Substituting the above expansions into Eqs. (5.13c) and (5.13f) gives:

$$\mathcal{F}_{0,2;\alpha} = -\frac{2n_0\tau k}{5(1-\alpha\tau)}\beta_{\alpha}, \quad \mathcal{F}_{1,2;\alpha} = \frac{2n_0\tau k}{5(1-\alpha\tau)}\left(\beta_{\alpha} + \frac{q_{\alpha}}{P_0}\right). \quad (5.18)$$

The moment method introduced in this section bears many similarities with the second-order hydrodynamics method discussed in Sec. IV. In particular, since the constitutive equations (5.14b) and (4.3b) for Π are the same in the two theories, Eqs. (4.10), (4.11) and (4.12) remain unchanged. The latter equation again can be solved either by setting $q_{\alpha} = -4P_0\beta_{\alpha}$

or by setting the square bracket to 0. In the latter case, the allowed values for α , namely $\alpha_{\eta,r}$ and $\alpha_{\eta,\pm}$ can be written as in Sec. IV B, being given in Eq. (4.19). For completeness, we reproduce these expressions here, specialised to the values of η , λ , τ_q and τ_{Π} given in Eq. (5.15):

$$\begin{aligned}\alpha_{\eta,r} &= \frac{1}{3\tau} \left[1 + \frac{1}{R_\eta} \left(1 - \frac{9k^2\tau^2}{5} \right) + R_\eta \right] \simeq \frac{1}{\tau} - \frac{4k^2\tau}{5} + O(\tau^3), \\ \alpha_{\eta,d} &= \frac{1}{3\tau} \left[1 - \frac{1}{2R_\eta} \left(1 - \frac{9k^2\tau^2}{5} \right) - \frac{R_\eta}{2} \right] \simeq \frac{4k^2\tau}{15} + O(\tau^3), \\ \alpha_{\eta,o} &= \frac{\sqrt{3}}{6\tau} \left[\frac{1}{R_\eta} \left(1 - \frac{9k^2\tau^2}{5} \right) - R_\eta \right] \simeq \frac{k}{\sqrt{3}} + O(\tau^2),\end{aligned}\tag{5.19}$$

where R_η (4.20) becomes:

$$R_\eta = \begin{cases} (1 - 3k\tau\sqrt{R_{\eta,\text{aux}}} + \frac{9}{5}k^2\tau^2)^{1/3}, & 0 < \tau < \tau_{\eta,\text{lim}}, \\ -(-1 + 3k\tau\sqrt{R_{\eta,\text{aux}}} - \frac{9}{5}k^2\tau^2)^{1/3}, & \tau > \tau_{\eta,\text{lim}}. \end{cases}\tag{5.20}$$

The function $R_{\eta,\text{aux}}$ (4.21) reduces to:

$$R_{\eta,\text{aux}} = 1 - \frac{18}{25}k^2\tau^2 + \frac{81}{125}k^4\tau^4.\tag{5.21}$$

Since the roots $\frac{1}{9}(5 \pm 10i)$ of $R_{\eta,\text{aux}}$ have a non-vanishing imaginary part and $R_{\eta,\text{aux}}(\tau = 0) = 1$, $R_{\eta,\text{aux}} > 0$ for all values of τ . The threshold value $\tau_{\eta,\text{lim}}$ defined in Eq. (4.22) and appearing in Eq. (5.20) is

$$\tau_{\eta,\text{lim}} = \frac{\sqrt{5}}{3k} \simeq 0.119.\tag{5.22}$$

When $q_\alpha = -4P_0\beta_\alpha$, Eq. (4.13) is replaced by:

$$\left[\frac{4\tau k^2}{3\alpha} - 4(1 - \alpha\tau) - \frac{16\tau^2 k^2}{15(1 - \alpha\tau)} \right] \beta_\alpha = 0.\tag{5.23}$$

The square bracket cancels when $\alpha \in \{\alpha_{\lambda,r}, \alpha_{\lambda,\pm}\}$, where we set $\alpha_{\lambda,\pm} = \alpha_{\lambda,d} \pm i\alpha_{\lambda,o}$. The exact expressions for the coefficients $\alpha_{\lambda,r}$, $\alpha_{\lambda,d}$ and $\alpha_{\lambda,o}$ read:

$$\begin{aligned}\alpha_{\lambda,r} &= \frac{1}{3\tau} \left[2 - \frac{1}{R_\lambda} \left(1 - \frac{9k^2\tau^2}{5} \right) - R_\lambda \right] \simeq \alpha_\lambda + O(\tau^3), \\ \alpha_{\lambda,d} &= \frac{1}{3\tau} \left[2 + \frac{1}{2R_\lambda} \left(1 - \frac{9k^2\tau^2}{5} \right) + \frac{R_\lambda}{2} \right] \simeq \frac{1}{\tau} - \frac{\alpha_\lambda}{2} + O(\tau^3), \\ \alpha_{\lambda,o} &= \frac{\sqrt{3}}{6\tau} \left[\frac{1}{R_\lambda} \left(1 - \frac{9k^2\tau^2}{5} \right) - R_\lambda \right] \simeq \frac{2k}{\sqrt{15}} + O(\tau^2),\end{aligned}\tag{5.24}$$

where $\alpha_\lambda = k^2\tau/3$ is defined in Eq. (3.8) and

$$R_\lambda = \begin{cases} \left[1 - \frac{6k\tau}{\sqrt{5}}\sqrt{R_{\lambda,\text{aux}}} + \frac{9k^2\tau^2}{10}\right]^{1/3}, & 0 < \tau < \tau_{\lambda,\text{lim}}^{\text{mom}}, \\ -\left[-1 + \frac{6k\tau}{\sqrt{5}}\sqrt{R_{\lambda,\text{aux}}} - \frac{9k^2\tau^2}{10}\right]^{1/3}, & \tau > \tau_{\lambda,\text{lim}}^{\text{mom}}, \end{cases} \quad (5.25)$$

In the above, $R_{\lambda,\text{aux}}$ is defined as:

$$R_{\lambda,\text{aux}} = 1 - \frac{99}{80}k^2\tau^2 + \frac{81}{100}k^4\tau^4 \quad (5.26)$$

Since the roots $\frac{5}{72}(11 \pm 3i\sqrt{15})$ are complex, $R_{\lambda,\text{aux}} > 0$ for all values of τ . The parameter $\tau_{\lambda,\text{lim}}^{\text{mom}}$ is defined as the value of τ at which the expression under the cubic root in Eq. (5.25) vanishes. It is given by

$$\tau_{\lambda,\text{lim}}^{\text{mom}} = \frac{\sqrt{5}}{3k}, \quad (5.27)$$

being identical to $\tau_{\eta,\text{lim}}$ (5.22). The definition (5.25) of R_λ ensures that the coefficients $\alpha_{\lambda,*}$ ($* \in \{r, d, o\}$), defined in Eq. (5.24), are real for all positive values of τ .

C. Longitudinal waves: solution

The solution can be split as in Eq. (4.24), i.e. $\widetilde{M} = \widetilde{M}_\lambda + \widetilde{M}_\eta$. In this case, the λ and η sectors of the solution have symmetric expressions, i.e.:

$$\begin{aligned} \widetilde{M}_\lambda &= M_{\lambda,r}e^{-\alpha_{\lambda,r}t} + (M_{\lambda,c}\cos\alpha_{\lambda,ot} + M_{\lambda,s}\sin\alpha_{\lambda,ot})e^{-\alpha_{\lambda,d}t}, \\ \widetilde{M}_\eta &= M_{\eta,r}e^{-\alpha_{\eta,r}t} + (M_{\eta,c}\cos\alpha_{\eta,ot} + M_{\eta,s}\sin\alpha_{\eta,ot})e^{-\alpha_{\eta,d}t}. \end{aligned} \quad (5.28)$$

The coefficients $M_{\times,*}$ (where $\times \in \{\lambda, \eta\}$ and $* \in \{r, c, s\}$) for $M \in \{\delta n, \mathcal{F}_{0,2}\}$ are

$$\begin{aligned} \delta n_{\times,r} &= kn_0 \frac{\beta_{\times,r}}{\alpha_{\times,r}}, & \mathcal{F}_{0,2;\times,r} &= -\frac{2kn_0\tau}{5} \frac{\beta_{\times,r}}{1 - \alpha_{\times,r}\tau}, \\ \delta n_{\times,c} &= kn_0 \frac{\alpha_{\times,d}\beta_{\times,c} + \alpha_{\times,o}\beta_{\times,s}}{\alpha_{\times,d}^2 + \alpha_{\times,o}^2}, & \delta n_{\times,s} &= kn_0 \frac{\alpha_{\times,d}\beta_{\times,s} - \alpha_{\times,o}\beta_{\times,c}}{\alpha_{\times,d}^2 + \alpha_{\times,o}^2}, \\ \mathcal{F}_{0,2;\times,c} &= -\frac{2kn_0\tau}{5} \frac{(1 - \alpha_{\times,d}\tau)\beta_{\times,c} - \alpha_{\times,o}\tau\beta_{\times,s}}{(1 - \alpha_{\times,d}\tau)^2 + (\alpha_{\times,o}\tau)^2}, \\ \mathcal{F}_{0,2;\times,s} &= -\frac{2kn_0\tau}{5} \frac{(1 - \alpha_{\times,d}\tau)\beta_{\times,s} + \alpha_{\times,o}\tau\beta_{\times,c}}{(1 - \alpha_{\times,d}\tau)^2 + (\alpha_{\times,o}\tau)^2}. \end{aligned} \quad (5.29)$$

On the λ sector, we also have

$$q_{\lambda,*} = -4P_0\beta_{\lambda,*}, \quad \mathcal{F}_{1,2;\lambda,*} = 3\mathcal{F}_{0,2;\lambda,*}, \quad \delta P_{\lambda,*} = \Pi_{\lambda,*} = 0. \quad (5.30)$$

On the η sector, we have

$$\delta P_{\eta,*} = \frac{4}{3}T_0\delta n_{\eta,*}, \quad \mathcal{F}_{1,2;\eta,*} = -\mathcal{F}_{0,2;\eta,*}, \quad \Pi_{\eta,*} = \frac{8}{3}T_0\mathcal{F}_{0,2;\eta,*}, \quad q_{\eta,*} = 0. \quad (5.31)$$

The initial conditions (2.23) and (4.30) refer only to $\widetilde{\beta}$, $\widetilde{\delta n}$, $\widetilde{\delta P}$, \widetilde{q} and $\widetilde{\Pi}$. In the moment approach considered in this section, the coefficients $\mathcal{F}_{0,2}$ and $\mathcal{F}_{1,2}$ are also free to evolve [in fact, they contribute only one degree of freedom, since $\Pi = 2T_0(\mathcal{F}_{0,2} - \frac{1}{3}\mathcal{F}_{1,2})$ is taken as an independent variable]. Since at $t = 0$, the system is initialised with the equilibrium distribution $f^{(\text{eq})}$, the initial conditions for $\mathcal{F}_{0,2}$ and $\mathcal{F}_{1,2}$ can be read from Eq. (5.10):

$$\widetilde{\mathcal{F}}_{0,2}(t=0) = 0, \quad \widetilde{\mathcal{F}}_{1,2}(t=0) = 0. \quad (5.32)$$

Imposing the initial conditions (2.23), (4.30) and (5.32) on the solution (5.28) yields the following solution for the integration constants $\beta_{\lambda,*}$:

$$\begin{aligned} \beta_{\lambda,r} &= \frac{\alpha_{\lambda,r}(1 - \alpha_{\lambda,r}\tau)(\alpha_{\lambda,d}^2 + \alpha_{\lambda,o}^2)}{4k[\alpha_{\lambda,o}^2 + (\alpha_{\lambda,d} - \alpha_{\lambda,r})^2]} \left(\frac{4\delta n_0}{n_0} - \frac{3\delta P_0}{P_0} \right), \\ \beta_{\lambda,s} &= \frac{\alpha_{\lambda,d}^2 + \alpha_{\lambda,o}^2}{4k\alpha_{\lambda,o}} \left(\frac{4\delta n_0}{n_0} - \frac{3\delta P_0}{P_0} \right) - \frac{\alpha_{\lambda,d}^2 + \alpha_{\lambda,o}^2 - \alpha_{\lambda,d}\alpha_{\lambda,r}}{\alpha_{\lambda,r}\alpha_{\lambda,o}} \beta_{\lambda,r}, \end{aligned} \quad (5.33)$$

while $\beta_{\lambda,c} = -\beta_{\lambda,r}$ and $\beta_{\eta,*}$ are the same as in Eq. (4.32b), obtained in the frame of the second order theory.

Since the integration constants $\beta_{\eta,*}$ obtained in the moment approach coincide with those obtained in the second order theory, the analytic solution for $\widetilde{\delta P}$ and $\widetilde{\Pi}$ is the same in these two approaches. Moreover, for the initial conditions corresponding to *Case 1* (i.e. $\delta n_0 = \delta P_0 = 0$), when $\beta_{\lambda,*} = 0$, the full analytic solution is identical in the moment approach and in the second order theory, being given in Eq. (4.34). We will therefore not analyse this case in this section. We will instead proceed to the analysis of *Case 2b* in the following subsection.

D. Numerical results (*Case 2b*)

Setting $\beta_0 = \delta P_0 = 0$ in Eq. (5.33) yields:

$$\begin{aligned} \beta_{\lambda,r} &= \frac{\alpha_{\lambda,r}(1 - \alpha_{\lambda,r}\tau)(\alpha_{\lambda,d}^2 + \alpha_{\lambda,o}^2)}{k[\alpha_{\lambda,o}^2 + (\alpha_{\lambda,d} - \alpha_{\lambda,r})^2]} \frac{\delta n_0}{n_0}, \\ \beta_{\lambda,s} &= \frac{\beta_{\lambda,r}}{\alpha_{\lambda,o}(1 - \alpha_{\lambda,r}\tau)} [\alpha_{\lambda,r} - \alpha_{\lambda,d} + (\alpha_{\lambda,d}^2 + \alpha_{\lambda,o}^2 - \alpha_{\lambda,d}\alpha_{\lambda,r})\tau], \end{aligned} \quad (5.34)$$

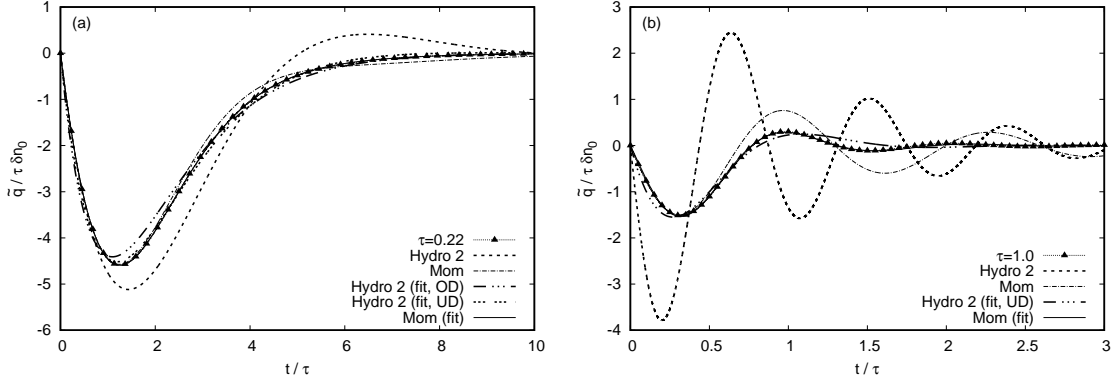


FIG. 13. Time evolution of $\tilde{q}/\tau\delta n_0$ at (a) $\tau = 0.22$ and (b) $\tau = 1.0$ for $\delta n_0 = 10^{-3}$. Since for the Chapman-Enskog value of λ_0 (3.3b) and $\tau_{q,0} = 1$ (4.5), in both cases $\tau > \tau_{\lambda,\text{lim}} \simeq 0.14$ (4.16), such that the curve corresponding to the second order hydrodynamics theory is given by the underdamped (UD) solution (4.36b). The analytic solution corresponding to the moment method is given in Eq. (5.36). The fitted curves are obtained as explained in Subsec. VD

while $\beta_{\lambda,c} = -\beta_{\lambda,r}$. Noting that $\tilde{\beta}_\eta = 0$, the heat flux is given simply by $\tilde{q} = -4P_0\tilde{\beta}$, while

$$\begin{aligned}\delta n_{\lambda,r} &= \delta n_0 \frac{(1 - \alpha_{\lambda,r}\tau)(\alpha_{\lambda,d}^2 + \alpha_{\lambda,o}^2)}{\alpha_{\lambda,o}^2 + (\alpha_{\lambda,d} - \alpha_{\lambda,r})^2}, \\ \delta n_{\lambda,c} &= \delta n_0 \alpha_{\lambda,r} \frac{(\alpha_{\lambda,d}^2 + \alpha_{\lambda,o}^2)\tau + \alpha_{\lambda,r} - 2\alpha_{\lambda,d}}{\alpha_{\lambda,o}^2 + (\alpha_{\lambda,d} - \alpha_{\lambda,r})^2} \delta n_0, \\ \delta n_{\lambda,s} &= \delta n_0 \frac{\alpha_{\lambda,r} \alpha_{\lambda,o}^2 + (\alpha_{\lambda,d} - \alpha_{\lambda,r})(\alpha_{\lambda,d}^2 + \alpha_{\lambda,o}^2)\tau - \alpha_{\lambda,d}}{\alpha_{\lambda,o}^2 + (\alpha_{\lambda,d} - \alpha_{\lambda,r})^2}.\end{aligned}\quad (5.35)$$

The full solution can be written as:

$$\begin{aligned}\tilde{\beta} &= \frac{\alpha_{\lambda,r}(\alpha_{\lambda,d}^2 + \alpha_{\lambda,o}^2)}{\alpha_{\lambda,o}^2 + (\alpha_{\lambda,d} - \alpha_{\lambda,r})^2} \frac{\delta n_0}{k n_0} \left\{ (1 - \alpha_{\lambda,r}\tau) e^{-\alpha_{\lambda,r}t} - [(1 - \alpha_{\lambda,r}\tau) \cos \alpha_{\lambda,o}t \right. \\ &\quad \left. - \frac{1}{\alpha_{\lambda,o}} [(\alpha_{\lambda,d}^2 + \alpha_{\lambda,o}^2 - \alpha_{\lambda,d}\alpha_{\lambda,r})\tau + \alpha_{\lambda,r} - \alpha_{\lambda,d}] \sin \alpha_{\lambda,o}t] e^{-\alpha_{\lambda,d}t} \right\}, \\ \widetilde{\delta n} &= \frac{\delta n_0}{\alpha_{\lambda,o}^2 + (\alpha_{\lambda,d} - \alpha_{\lambda,r})^2} \left\{ (1 - \alpha_{\lambda,r}\tau)(\alpha_{\lambda,d}^2 + \alpha_{\lambda,o}^2) e^{-\alpha_{\lambda,r}t} \right. \\ &\quad \left. + \alpha_{\lambda,r} \left([(\alpha_{\lambda,d}^2 + \alpha_{\lambda,o}^2)\tau + \alpha_{\lambda,r} - 2\alpha_{\lambda,d}] \cos \alpha_{\lambda,o}t \right. \right. \\ &\quad \left. \left. + \frac{1}{\alpha_{\lambda,o}} \{ \alpha_{\lambda,o}^2 + (\alpha_{\lambda,d} - \alpha_{\lambda,r}) [(\alpha_{\lambda,d}^2 + \alpha_{\lambda,o}^2)\tau - \alpha_{\lambda,d}] \} \sin \alpha_{\lambda,o}t \right) e^{-\alpha_{\lambda,d}t} \right\}, \\ \tilde{q} &= -4P_0\tilde{\beta}.\end{aligned}\quad (5.36)$$

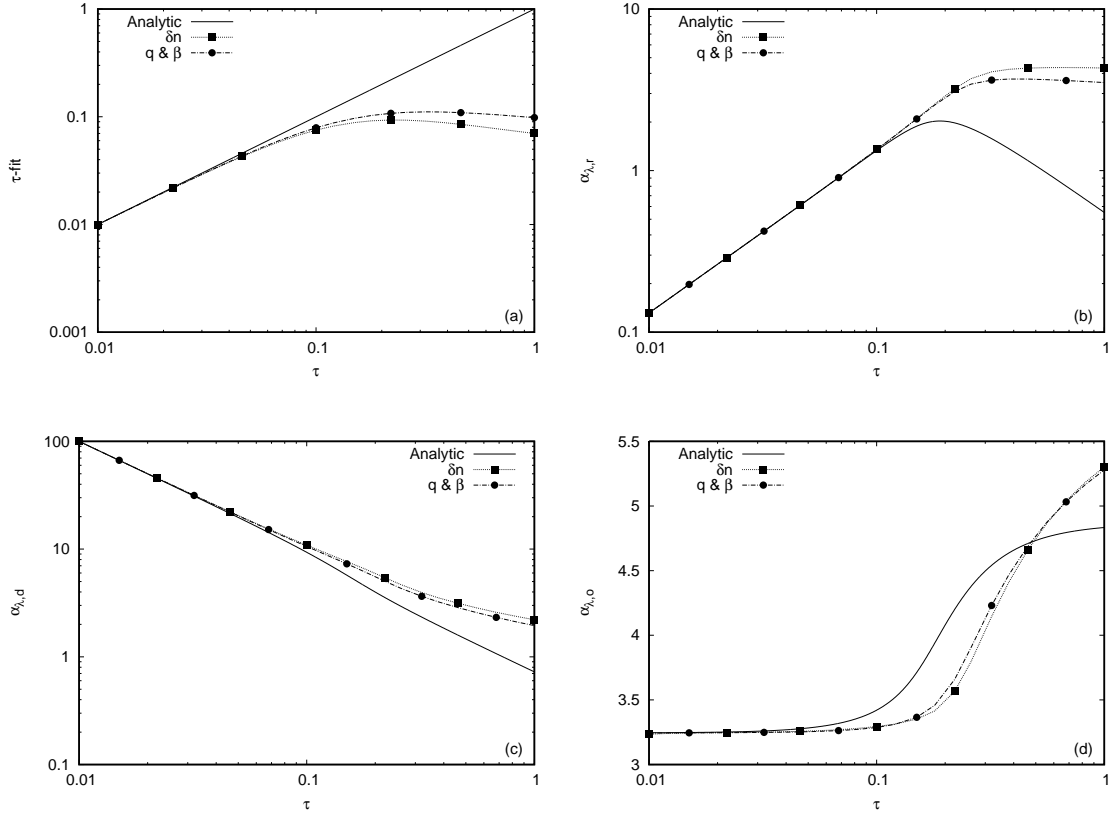


FIG. 14. Analysis with respect to τ of (a) the parameter τ , (b) $\alpha_{\lambda,r}$, (c) $\alpha_{\lambda,d}$ and (d) $\alpha_{\lambda,o}$ for the initial conditions of *Case 2b* (i.e. $\beta_0 = \delta P_0 = 0$ and $\delta n_0 = 10^{-3}$). The analytic curves are given by Eq. (5.24) in (b)–(d), while in (a), the analytic curve represents τ . The numerical curves shown with dotted lines and symbols are obtained by performing a nonlinear fit, as described in Subsec. VD.

The functional form of \tilde{q} obtained using the moment method is more convenient to use than the one given in the second order hydrodynamics case (4.36), since in the former case, there is no distinction between the overdamped and the underdamped regimes. In Fig. 13, we test the validity of the solution (5.36) for \tilde{q} at $\tau = 0.22$ and $\tau = 1.0$. Since, according to Eq. (4.16), $\tau > \tau_{\lambda,\text{lim}} \simeq 0.14$ (the Chapman-Enskog value $\lambda_0 = 4/3$ and $\tau_{q,0} = 1$ were used), Eq. (4.36b) is used to represent the analytic solution obtained in the frame of the second order hydrodynamics theory. At $\tau = 0.22$, the solution corresponding to the moments method is much closer to the numerical result than the second order hydrodynamics one. When $\tau = 1.0$, both theories give solutions which deviate considerably from the numerical results. In this regime, we can further test the validity of the functional form of the analytic

solutions discussed above. In the second order hydrodynamics case, we perform a nonlinear fit of the solutions (4.36a) and (4.36b) by considering the coefficients $\alpha_{\lambda,d}$ and $\alpha_{\lambda,o}$ ($\bar{\alpha}_{\lambda,d}$ and $\bar{\alpha}_{\lambda,o}$) as free parameters. Fig. 13 shows that, at $\tau = 0.22$, the fit corresponding to the overdamped form (4.36a) is less accurate than the fit corresponding to the underdamped form (4.36b). At $\tau = 1.0$, the fit corresponding to the UD form also starts to present visible deviations from the numerical result. In the moment method solution (5.36), the nonlinear fit is performed by considering τ , $\alpha_{\lambda,r}$, $\alpha_{\lambda,d}$ and $\alpha_{\lambda,o}$ as free parameters. The resulting fit is in much better agreement with the numerical results.

Let us now consider the τ dependence of the coefficients τ , $\alpha_{\lambda,r}$, $\alpha_{\lambda,d}$ and $\alpha_{\lambda,o}$ as obtained by performing a nonlinear fit of Eq. (5.36) to the numerical data. Figure 14(a) shows that $\tau - \text{fit}$ [i.e., the best fit value for the parameter τ appearing in Eq. (5.36)] depends non-monotonically on τ , i.e. it reaches a maximum value around $\tau \simeq 0.22$ and $\tau \simeq 0.32$ when considering the evolution of $\widetilde{\delta n}$ and \widetilde{q} , respectively, after which it decreases with τ .

The analytic expression for $\alpha_{\lambda,r}$ (5.24), represented using a continuous line in Fig. 14(b), reduces at small values of τ to α_λ (3.8) defined within the first order theory. While the first order theory predicts a linear increase of α_λ with τ , the moment method predicts a maximum of $\alpha_{\lambda,r}$ at $\tau \simeq 1.19/k \simeq 0.19$, after which it decreases according to the asymptotic behaviour $\lim_{\tau \rightarrow \infty} \alpha_{\lambda,r} = 5/9\tau$. The fitted values also are non-monotonic, exhibiting a slight decreasing trend when $\tau \gtrsim 0.38$ in the case of \widetilde{q} and $\widetilde{\beta}$ and $\tau \gtrsim 0.68$ when the nonlinear fit is performed on $\widetilde{\delta n}$.

The coefficient $\alpha_{\lambda,d}$ is analysed in Fig. 14(c). The analytic expression (5.24) predicts a monotonic decrease of $\alpha_{\lambda,d}$. The curve corresponding to the nonlinear fit also decreases monotonically over the range of τ considered in Fig. 14(c), but at a lesser rate compared to the analytic prediction.

Finally, the oscillation frequency $\alpha_{\lambda,o}$ (which has no analogue in the first order theory) is represented in Fig. 14(d). It can be seen that both the analytic and the numerical curves indicate that $\alpha_{\lambda,o}$ starts to increase when $\tau \gtrsim 0.1$.

E. Summary

In this section, we employed a moment-based method to study the attenuation of a longitudinal wave. We obtain the moment equations by projecting the distribution function

f on the space of the generalised Laguerre and Legendre polynomials. We immediately find the same expressions for the transport coefficients as those obtained through the Chapman-Enskog expansion. The difference between our approach and the traditional Grad moment method introduced by Israel and Steward [10] is that the truncation of f is performed with respect to orthogonal polynomials, while in the latter approach, a nonorthogonal polynomial basis is employed [28]. In this sense, our approach is similar to that employed in Ref. [28].

The minimal set of moment equations which gives access to the evolution of the macroscopic four-flow N^μ and stress-energy tensor $T^{\mu\nu}$ is obtained by retaining in the expansion of f the zeroth and first orders with respect to p (expanded using generalised Laguerre polynomials) and zeroth, first and second orders with respect to ξ (expanded using Legendre polynomials). The system contains 6 equations for the five hydrodynamic variables δn , β , δP , q and Π , as well as for a non-hydrodynamic variable not present in the theory of second order hydrodynamics.

The solution of the set of moment equations is identical on the shear stress sector with the one obtained from the second order hydrodynamics equations discussed in Sec. IV. On the heat flux sector, the second-order hydrodynamics solution is improved in the moment method approach, where the functional form of q allows for a smooth transition from the overdamped to the underdamped regimes highlighted in Sec. IV E. Furthermore, the range of validity of the analytical solution of the moment equations is larger than the one corresponding to the second-order hydrodynamics equations. Moreover, the functional form of the former can be fitted to the numerical data with remarkable accuracy even at $\tau = 1$.

VI. THE BALLISTIC LIMIT

We end our analysis of the longitudinal wave problem by considering the free-streaming limit. In this case, the relativistic Boltzmann equation (2.1) reduces to:

$$\partial_t f + \xi \partial_z f = 0, \quad (6.1)$$

where $\xi = p^z/p$. The solution of Eq. (6.1) is $f(z, \xi, t) = f(z - \xi t)$, subject to the following initial condition:

$$f(z, \xi, t = 0) = \frac{n(z)}{8\pi T^3(z)} \exp \left\{ -\frac{p\gamma(z)}{T(z)} [1 - \xi \beta(z)] \right\}. \quad (6.2)$$

We now consider the case of the longitudinal wave, where:

$$\begin{aligned} n(z, t = 0) &= n_0 + \delta n_0 \cos kz, & P(z, t = 0) &= P_0 + \delta P_0 \cos kz, \\ \beta(z, t = 0) &= \beta_0 \sin kz. \end{aligned} \quad (6.3)$$

Assuming that δn_0 , δP_0 and β_0 are small, Eq. (6.2) can be linearised as follows:

$$\begin{aligned} f(z, \xi, t = 0) &\simeq \frac{n_0}{8\pi T_0^3} e^{-p/T_0} \left\{ 1 + \frac{p\xi}{T_0} \beta_0 \sin kz \right. \\ &\quad \left. + \left[\frac{4\delta n_0}{n_0} - \frac{3\delta P_0}{P_0} + \frac{p}{T_0} \left(\frac{\delta P_0}{P_0} - \frac{\delta n_0}{n_0} \right) \right] \cos kz \right\}. \end{aligned} \quad (6.4)$$

The solution at $t > 0$ is given by replacing the product kz in Eq. (6.4) by $k(z - \xi t)$.

We are interested in tracking the time evolution of the macroscopic quantities n , P , β , q and Π . These can be obtained from N^μ and $T^{\mu\nu}$ (2.3), which reduce to:

$$\begin{aligned} N^\mu(t, z) &= \int_0^\infty dp p^2 \int d\Omega v^\mu f(z - \xi t), \\ T^{\mu\nu}(t, z) &= \int_0^\infty dp p^3 \int d\Omega v^\mu v^\nu f(z - \xi t), \end{aligned} \quad (6.5)$$

where $v^\mu = p^\mu/p = (1, \sin \theta \cos \varphi, \sin \theta \sin \varphi, \cos \theta)$. The result is:

$$\begin{aligned} \widetilde{\delta n} &= \delta n_0 \frac{\sin kt}{kt} + 3\beta_0 n_0 \left[\frac{\cos kt}{kt} - \frac{\sin kt}{(kt)^2} \right], \\ \widetilde{\delta P} &= \delta P_0 \frac{\sin kt}{kt} + 4P_0 \beta_0 \left[\frac{\cos kt}{kt} - \frac{\sin kt}{(kt)^2} \right], \\ \widetilde{\beta} &= -\frac{\delta n_0}{n_0} \left[\frac{\cos kt}{kt} - \frac{\sin kt}{(kt)^2} \right] \\ &\quad + 3\beta_0 \left[\frac{\sin kt}{kt} + \frac{2 \cos kt}{(kt)^2} - \frac{2 \sin kt}{(kt)^3} \right], \\ \widetilde{q} &= P_0 \left(\frac{4\delta n_0}{n_0} - \frac{3\delta P_0}{P_0} \right) \left[\frac{\cos kt}{kt} - \frac{\sin kt}{(kt)^2} \right], \\ \widetilde{\Pi} &= 2\delta P_0 \left[\frac{\sin kt}{kt} + \frac{3 \cos kt}{(kt)^2} - \frac{3 \sin kt}{(kt)^3} \right] \\ &\quad + 8P_0 \beta_0 \left[\frac{\cos kt}{kt} - \frac{4 \sin kt}{(kt)^2} - \frac{9 \cos kt}{(kt)^3} + \frac{9 \sin kt}{(kt)^4} \right]. \end{aligned} \quad (6.6)$$

The leading order term in all of the above expressions is damped according to a factor of t^{-1} .

Figure 15 illustrates the close agreement between our numerical method and the analytic solution (6.6) when $k = 2\pi/L$ and $L = 1$. Each plot in Fig. 15 contains three curves

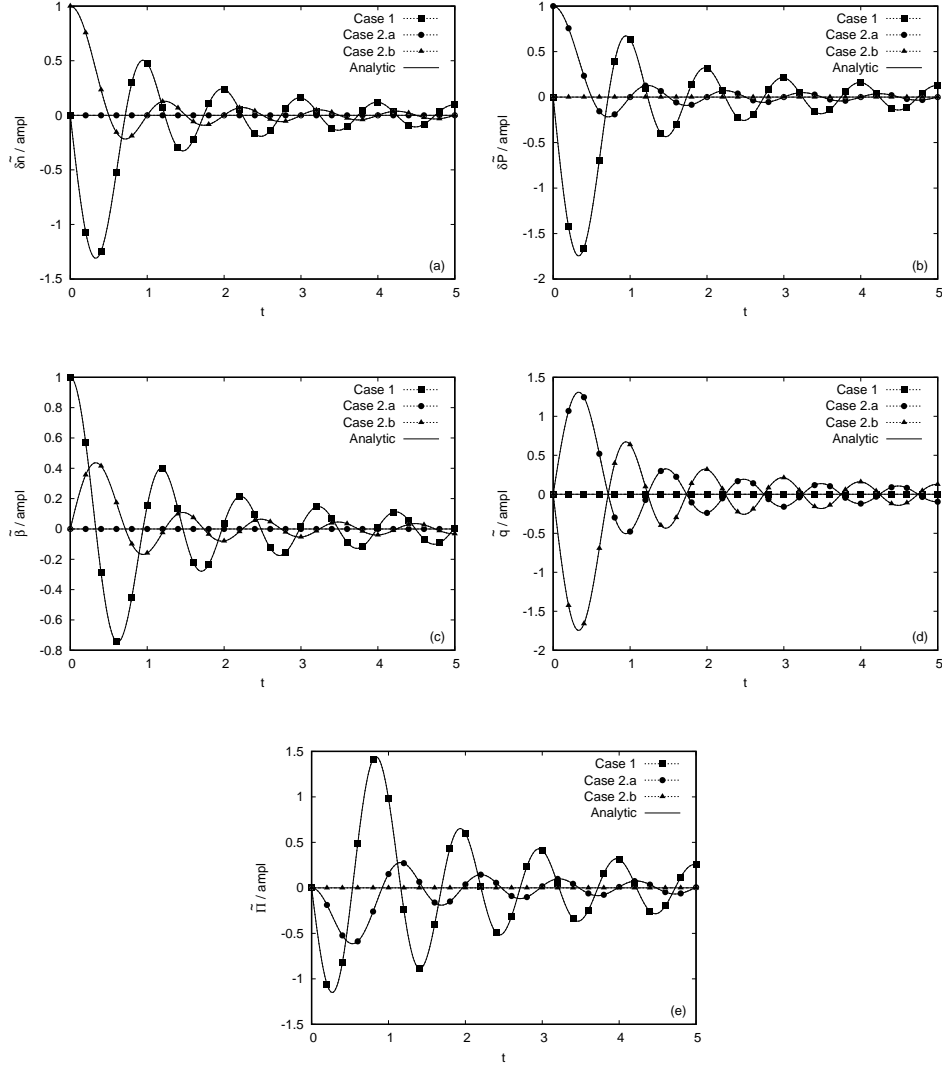


FIG. 15. Time evolution of (a) $\widetilde{\delta n}$, (b) $\widetilde{\delta P}$, (c) $\widetilde{\beta}$, (d) \widetilde{q} and (e) $\widetilde{\Pi}$ in the free-streaming regime, normalised with respect to the wave amplitude. The system is initialised with the following initial conditions: *Case 1*: $\delta n_0 = \delta P_0 = 0$ and the wave amplitude is $\beta_0 = 10^{-3}$; *Case 2(a)*: $\delta n_0 = \beta_0 = 0$ and the wave amplitude is $\delta P_0 = 10^{-3}$; *Case 2(b)*: $\delta P_0 = \beta_0 = 0$ and the wave amplitude is $\delta n_0 = 10^{-3}$, such that the wave amplitude is always 10^{-3} . The numerical results are represented with dashed lines and points, while the analytic results corresponding to Eq. (6.6) are represented using solid lines. The analytic and numerical curves are indistinguishable.

corresponding to the initial conditions described in *Cases 1* ($\delta n_0 = \delta P_0 = 0$, $\beta_0 = 10^{-3}$), *2(a)* ($\delta n_0 = \beta_0 = 0$, $\delta P_0 = 10^{-3}$) and *2(b)* ($\delta P_0 = \beta_0 = 0$, $\delta n_0 = 10^{-3}$). The plots illustrate the time evolution of $\widetilde{\delta n}$, $\widetilde{\delta P}$, $\widetilde{\beta}$, \widetilde{q} and $\widetilde{\Pi}$, where our numerical results are represented with

dashed lines and points, while the analytic expressions (6.6) are represented using solid lines. The quantities on the vertical axis are divided by the amplitude of the perturbation, namely β_0 for *Case 1*, δP_0 for *Case 2(a)* and δn_0 for *Case 2(b)*. For simplicity, the amplitude was taken equal to 10^{-3} in all cases. It can be seen that the agreement between our numerical results and the analytic expressions is excellent.

Each plot in Fig. 15 displays two non-trivial curves and a line corresponding to a vanishing value. This is because all of the expressions in Eq. (6.6) have on the right hand side only two terms, e.g. $\widetilde{\delta n}$ vanishes when $\delta n_0 = \beta_0 = 0$ for all values of δP_0 , etc. It is worth pointing out that $\widetilde{\delta P}$ and $\widetilde{\Pi}$ vanish when $\beta_0 = \delta P_0/P_0 = 0$, as also predicted by the second-order hydrodynamics theory discussed in Sec. IV, as well as by the moment method presented in Sec. V.

A fundamental difference between the hydrodynamic and the free-streaming regimes is that the attenuation of the wave perturbation in the former case is exponential (dissipative), while in the latter case, it is of the form t^{-1} (dispersive).

VII. CONCLUSION AND OUTLOOK

In this paper, we studied the attenuation of a longitudinal wave in a medium formed of ultrarelativistic (massless) particles from the following perspectives: the first- and second-order hydrodynamics equations, the moment method, the free-streaming regime and by employing the numerical method introduced in Ref. [20]. In our investigations, we considered the linearised limit of the hydrodynamics equations, which can be solved analytically. The analytic solutions were confronted with the numerical results in order to highlight the properties of the transport coefficients (and relaxation times in the second order hydrodynamics and moment-method cases) in this system, for three particular cases: in *Case 1*, the initial density and pressure perturbations vanish ($\delta n_0/n_0 = \delta P_0/P_0 = 0$); in *Case 2a*, the initial density and velocity perturbations vanish ($\delta n_0/n_0 = \beta_0 = 0$); finally, in *Case 2b*, the initial pressure and velocity perturbations vanish ($\delta P_0/P_0 = \beta_0 = 0$). Since in *Case 1*, the flow is adiabatic (i.e. the heat flux vanishes at all times) for all tested values of the initial wave perturbation β_0 , we considered this case for the study of the shear viscosity η by following the attenuation of the density, velocity, pressure and shear pressure perturbations. We considered *Case 2a* and *Case 2b* to study the heat conductivity λ by following

the attenuation of the heat flux.

Throughout this paper, we have performed two types of tests: (a) we compared the time evolution of the amplitudes $\widetilde{\delta n}$, $\widetilde{\delta P}$, $\widetilde{\beta}$, \widetilde{q} and $\widetilde{\Pi}$ of the wave perturbations obtained from the numerical simulations with the analytic predictions corresponding to the Chapma-Enskog and Grad expressions for the transport coefficients; and (b), we performed nonlinear numerical fits of these analytic expressions to the numerical results by considering the transport coefficients as fitting parameters. The analytic solutions for the evolution of the amplitudes were considered in terms of the modes allowed by the hydrodynamic equations.

In the first-order theory, three modes were highlighted: an evanescent mode (corresponding to the dampening coefficient α_λ) and two modes undergoing oscillatory attenuation described by the dampening coefficient α_d and the oscillation angular frequency α_o . Since there is no contribution to the heat flux from the oscillatory modes, the evanescent mode can be regarded as describing the heat flux sector (also, α_λ is determined exclusively in terms of the heat conductivity λ). Conversely, the oscillatory modes describe the shear pressure sector, since α_d and α_o depend only on the shear viscosity η . Thus, the numerical fits of $\widetilde{\delta n}$, $\widetilde{\beta}$, $\widetilde{\delta P}$ and $\widetilde{\Pi}$ were performed by considering α_d and α_o as free parameters, while α_λ was considered as a free parameter during the nonlinear fit of the expression for \widetilde{q} to the numerical data.

In the analysis based on the second-order hydrodynamics equations, the heat flux sector is described by two modes ($\alpha_{\lambda,d}$ and $\alpha_{\lambda,o}$) which are evanescent for $\tau < \tau_{q,\text{lim}}$, while for $\tau > \tau_{q,\text{lim}}$, their attenuation is oscillatory. The coefficients $\alpha_{\lambda,d}$ and $\alpha_{\lambda,o}$ now depend on λ and also on the heat flux relaxation time τ_q . The shear pressure sector is also enlarged by the addition of an evanescent mode corresponding to the dampening coefficient $\alpha_{\eta,r}$, while the other two modes describe an oscillatory attenuation with dampening coefficient $\alpha_{\eta,d}$ and angular frequency $\alpha_{\eta,o}$. These three coefficients depend on η , as well as on the shear pressure relaxation time τ_Π . The nonlinear fit of the heat flux was performed by considering $\alpha_{\lambda,d}$ and $\alpha_{\lambda,o}$ as free parameters with the expression of \widetilde{q} written in both the evanescent (overdamped, OD) and in the oscillatory (underdamped, UD) forms. The nonlinear fits of the other amplitudes was performed by considering $\alpha_{\eta,*}$ ($* \in \{r, d, o\}$) as free parameters, as well as a fourth parameter (τ_Π for $\widetilde{\delta n}$, $\widetilde{\delta P}$ and $\widetilde{\beta}$ and the ratio η/τ_Π for $\widetilde{\Pi}$), which was considered as a free parameter due to the mathematical form of the analytic solution.

Finally, in the case of the moment-based method, the shear pressure sector was found

to be identical to that obtained within the second-order hydrodynamics approach. Due to the addition of a sixth (non-hydrodynamic) mode, the heat flux sector was enlarged by the addition of a purely evanescent mode damped by the coefficient $\alpha_{\lambda,r}$, while the other two modes are of oscillatory type, damped by the coefficient $\alpha_{\lambda,d}$ and having oscillation frequency $\alpha_{\lambda,o}$. In comparison to the second order hydrodynamics result, this solution behaves as nearly evanescent at small values of τ , since $\alpha_{\lambda,d} \sim \tau^{-1}$ quickly suppresses the oscillatory contributions. At larger values of τ , the oscillatory modes contribute significantly to the time evolution of \tilde{q} , which explains the better agreement to the numerical data observed at large values of τ . The nonlinear fit of \tilde{q} in the case of the moment method was performed by considering $\alpha_{\lambda,*}$ ($* \in \{r, d, o\}$) and τ as free parameters. The nonlinear fit of $\tilde{\Pi}$ was performed by considering $\alpha_{\eta,*}$ ($* \in \{r, d, o\}$) and τ as free parameters.

Both tests described above support the conclusion that, at small values of the Anderson-Witting relaxation time τ (typically, $\tau \lesssim 0.05$), the expressions for the first order transport coefficients (λ and η) corresponding to the Anderson-Witting collision term are those predicted through the Chapman-Enskog procedure, which differ from the expressions obtained using Grad's 14 moment approach. This conclusion is supported by various evidence in the literature [7, 8, 11–14, 20, 23]. Also, we were able to confirm the well-known results that the relaxation times for the shear pressure τ_{Π} and heat flux τ_q are exactly equal to τ . These results were also obtained analytically when we considered constructing the solution of the AWB equation using a moment-based method. As remarked in Ref. [28], our method is capable of reproducing the Chapman-Enskog transport coefficients since the distribution function is expanded with respect to orthogonal polynomials, while in the standard Grad method, the expansion is performed with respect to the nonorthogonal basis consisting of powers of the particle momentum p^μ .

By performing the test (a), we were able to highlight that the analytic solution obtained using the first-order hydrodynamics theory loses applicability when $\tau \gtrsim 0.05$. Since the constitutive equations for the heat flux and shear pressure tensor do not allow initial conditions to be specified for these fields, the first order approximation is always inaccurate for a time scale $t \simeq 5\tau$. On this interval, the solution of the second-order hydrodynamics equations reproduce with good accuracy the numerical results for $\tau \lesssim 0.1$. While the evolution of the amplitude of the shear pressure $\tilde{\Pi}$ is the same within the frames of the second-order hydrodynamics and the moment-based method considered in this paper, our numerical experiments

show that the evolution of the heat flux amplitude \tilde{q} is better captured by the moment method, which offers a reasonable agreement with the numerical results up to $\tau \simeq 0.22$.

We further considered the viability of the functional form of the analytic solutions obtained using the various hydrodynamic theories described above. To this end, we performed the nonlinear fits corresponding to test (b) and analysed the results in three ways, described below.

First, we considered a comparison between the numerical results for \tilde{q} and $\tilde{\Pi}$ and their analytic expressions corresponding to the best-fit values of the free parameters. At $\tau = 0.26$, we highlighted that the analytic expression for $\tilde{\Pi}$ obtained using the second-order hydrodynamics theory (also from the moment-based method) was indistinguishable from the numerical results when the best-fit values of $\alpha_{\eta,*}$ and τ_{Π} were used, compared to the analytic prediction for these coefficients. The improvement of the analytic expression obtained using the first-order hydrodynamics equations was not significant, since this expression does not permit the value of $\tilde{\Pi}$ to be fixed at $t = 0$. In the case of the heat flux, the moment-based method provided a much more robust analytic expression for \tilde{q} , which could be fitted remarkably well to the numerical results even at $\tau = 1$, while the solution obtained within the second-order hydrodynamics formulation corresponding to the best fit parameters was in visible disagreement compared to the numerical result, although the overall evolution was still in reasonable agreement with the numerical data.

We further considered the dependence on τ of the free parameters used in the nonlinear fitting procedure. In all approaches, the dampening coefficient of the oscillatory modes on the shear pressure sector (α_{η} in the first-order theory, $\alpha_{\eta,d}$ in the second-order theory and in the moment-based approach) was predicted analytically to grow (almost) linearly with τ . However, the numerical fits indicate that this coefficient increases at a much slower rate when $\tau \gtrsim 0.05$. A similar behaviour was highlighted for the coefficient governing the evanescent mode on the heat flux sector (α_{λ} in the first order theory, $\alpha_{\lambda,-}$ in the second order theory and $\alpha_{\lambda,r}$ in the moment-based method). Thus, our analysis indicates that the hydrodynamic theories considered in this paper break down when $\tau \gtrsim 0.05$.

Next, we performed a similar analysis of the dependence of the best fit parameters with respect to the wave amplitude at fixed $\tau = 0.0083$. We found significant deviations from the analytic predictions when the amplitude (β_0 for *Case 1*, $\delta P_0/P_0$ for *Case 2a* and $\delta n_0/n_0$ for *Case 2b*) became larger than ~ 0.05 , indicating the inapplicability of the analysis in the

linearised approximation at wave amplitudes larger than this value.

In order to gain some insight on the reason for the failure of the hydrodynamic theories to describe the attenuation of the longitudinal wave at larger values of τ , we investigated the ballistic (free molecular flow) limit of this problem. In this case, the analytic solution for the distribution function f indicates that the attenuation of the longitudinal wave is dispersive (i.e. the dampening is polynomial in t^{-1}) instead of dissipative (i.e. there is no exponential dampening). This behaviour was exactly recovered numerically, confirming the applicability of our numerical method in this regime. Thus, the solution of the hydrodynamics equations cannot describe correctly the attenuation of the longitudinal wave in the transition regime, where the dispersive component becomes important, since the functional form of these solutions does not include terms which are polynomial in t^{-1} .

Finally, we mention the particular case when at initial time, the velocity and pressure perturbations of the wave vanish, i.e. $\beta_0 = \delta P_0 = 0$. In this case, the pressure and shear pressure remain constant in time and the attenuation of the density, velocity and heat flux is purely evanescent (i.e. non-oscillatory). While the second-order hydrodynamics theory and the moment method recovered exactly this behaviour, the first-order theory always predicted an oscillatory attenuation of all variables (including the pressure and shear pressure, but excluding the heat flux), where the amplitude of the oscillations is of the same order of magnitude as the evanescent component. The above behaviour persists at small values of τ (we performed the tests with $\tau = 0.0083$), indicating a fundamental flaw of the first-order hydrodynamics equations.

ACKNOWLEDGEMENTS

The author would like to thank Prof. Amaresh Jaiswal for useful discussions. This work was supported by a grant of the Romanian National Authority for Scientific Research and Innovation, CNCS-UEFISCDI, project number PN-II-RU-TE-2014-4-2910.

Appendix A: Numerical method

In order to solve the AWB equation (2.1), we employ the relativistic spherical lattice Boltzmann (R-SLB) models introduced in Ref. [20] as an extension of the non-relativistic

spherical lattice Boltzmann (SLB) models introduced in Ref. [44]. A number of $N = 100$ nodes are chosen along the z axis, where periodic boundary conditions apply, while the flow is assumed to be homogeneous along the x and y directions. The advection and time evolution are performed using the fifth-order weighted essentially non-oscillatory (WENO-5) [32] and third-order TVD Runge-Kutta (RK-3) [39] schemes, as presented in Ref. [20]. The lattice spacing is $\delta z = 10^{-2}$. The time step was set to $\delta t = 10^{-3}$ for the analysis performed within the frame of the first-order hydrodynamics theory in Sec. III. In the case of the second-order hydrodynamics theory and moment-based method considered in Secs. IV and V, we employed a time step $\delta t = 10^{-4}$ to allow an increased temporal resolution (i.e. more data points) for the study of the early time evolution of the longitudinal wave.

The momentum space is factorised using spherical coordinates p , θ and φ , which are discretised using Q_L , Q_ξ and Q_φ quadrature points, respectively. The quadrature order along the p direction is set to $Q_L = 2$, while the azimuthal quadrature order is $Q_\varphi = 1$. The model thus employs $Q_L \times Q_\xi \times Q_\varphi = 2Q_\xi$ velocities.

The value of Q_ξ is chosen depending on the value of the relaxation time τ . As discussed in Ref. [20], $Q_\xi = 6$ is sufficient to obtain accurate results at $\tau < 0.01$. For values of τ between 0.01 and 0.1, we set $Q_\xi = 20$, while for $\tau \geq 0.1$, we chose $Q_\xi = 200$.

The system is initialised with an equilibrium distribution $f^{(\text{eq})}$ (2.2) at each point $z_\ell = -0.5 + (\ell - \frac{1}{2})\delta z$, truncated to $N_L = 1$ and $N_\Omega = 5$ with respect to p and $\xi = \cos \theta$, as explained in Ref. [20].

At a later time $t_s = s \delta t$ ($s = 1, 2, \dots T$), the quantities with tilde defined in Eqs. (2.20) are obtained as:

$$\begin{pmatrix} \widetilde{\beta}_s \\ \widetilde{q}_s \end{pmatrix} = 2\delta z \sum_{\ell=1}^N \begin{pmatrix} \beta_{s,\ell} \\ q_{s,\ell} \end{pmatrix} \sin kz_\ell, \\ \begin{pmatrix} \widetilde{\delta n}_s \\ \widetilde{\delta P}_s \\ \widetilde{\Pi}_s \end{pmatrix} = 2\delta z \sum_{\ell=1}^N \begin{pmatrix} n_{s,\ell} - n_0 \\ P_{s,\ell} - P_0 \\ \Pi_{s,\ell} \end{pmatrix} \cos kz_\ell. \quad (\text{A1})$$

In the case of the analysis using the first-order theory, performed in Sec. III, $T = 20.000$ and the resulting values $\widetilde{\beta}_s$, etc. are stored at intervals of $10\delta t = 0.01$ resulting in a number of 2.000 values which were further processed using MathematicaTM to obtain a nonlinear fit, based on the analytic solution for the flow, as described in Secs. III C and III D. Since in the

nonlinear theory, q and Π cannot be imposed at initial time, the analytic expression for the evolution of \tilde{q} and $\tilde{\Pi}$ is not accurate at small values of t . We thus always ignored the first 50 points (i.e. up to $t = 0.5$) in the data sets when performing the nonlinear fits for these quantities.

In the case of the analysis using the second-order theory and the moment method, performed in Secs. IV and V, respectively, the values of the field amplitudes $\tilde{\beta}_s$, etc. were stored at intervals of $\delta t = 10^{-4}$. The value of T was obtained using the following algorithm. For $0.001 \leq \tau \leq 0.1$, we considered a number of time steps equal to $T = 100(\tau/\delta t)$ (i.e. up to $t = 100\tau$). This ensured a balanced coverage of the initial stage corresponding to the relaxation of the nonequilibrium parameters \tilde{q} and $\tilde{\Pi}$ from their initial vanishing values towards the values predicted by the first order theory (up to $t \sim 5\tau$), as well as of the later stage of the wave evolution, where the attenuation effects dominate. For $0.1 < \tau < 0.32$, we chose a number of $T = 1/(\tau\delta t)$ points (i.e. corresponding to $t \simeq \tau^{-1}$), while for all $\tau \geq 0.32$, we performed $T = 32.000$ time steps (i.e. up to $t = 3.2$).

-
- [1] C. Cercignani and G. M. Kremer, The relativistic Boltzmann equation: theory and applications (Birkhäuser Verlag, Basel, Switzerland, 2002).
 - [2] C. Marle, Annales de l'I.H.P. Physique théorique **10**, 67–126 (1969) .
 - [3] J. L. Anderson and H. R. Witting, Physica **74**, 466–488 (1974).
 - [4] J. L. Anderson and H. R. Witting, Physica **74**, 489–495 (1974).
 - [5] P. L. Bhatnagar, E. P. Gross, and M. Krook, Phys. Rev. **94**, 511–525 (1954).
 - [6] J. D. Bjorken, Phys. Rev. D **27**, 140–151 (1983).
 - [7] W. Florkowski, R. Ryblewski, and M. Strickland, Phys. Rev. C **88**, 024903 (2013).
 - [8] W. Florkowski, R. Ryblewski, and M. Strickland, Nucl. Phys. A **916**, 249–259 (2013).
 - [9] W. Florkowski, E. Maksymiuk, R. Ryblewski, and M. Strickland, Phys. Rev. C **89**, 054908 (2014).
 - [10] W. Israel and J. M. Stewart, Ann. Phys. **118**, 341–372 (1979).
 - [11] W. Florkowski, A. Jaiswal, E. Maksymiuk, R. Ryblewski, and M. Strickland, Phys. Rev. C **91**, 054907 (2015).
 - [12] R. Ryblewski, J. Phys.: Conf. Ser. **612**, 012058 (2015).

- [13] G. S. Denicol, S. Jeon, and C. Gale, Phys. Rev. C **90**, 024912 (2014).
- [14] R. S. Bhalerao, A. Jaiswal, S. Pal, and V. Sreekanth, Phys. Rev. C **89**, 054903 (2014).
- [15] M. Mendoza, B. M. Boghosian, H. J. Herrmann, and S. Succi, Phys. Rev. Lett. **105**, 014502 (2010).
- [16] P. Romatschke, M. Mendoza, and S. Succi, Phys. Rev. C **84**, 034903 (2011).
- [17] D. Hupp, M. Mendoza, I. Bouras, S. Succi, and H. J. Herrmann, Phys. Rev. D **84**, 125015 (2011).
- [18] F. Mohseni, M. Mendoza, S. Succi, and H. J. Herrmann, Phys. Rev. D **87**, 083003 (2013).
- [19] M. Mendoza, I. Karlin, S. Succi, and H. J. Herrmann, Phys. Rev. D **87**, 065027 (2013).
- [20] R. Blaga and V. E. Ambruş, arXiv:1612.01287 [physics.flu-dyn].
- [21] R. Blaga and V. E. Ambruş, AIP Conf. Proc. **1796**, 020010 (2017).
- [22] A. Gabbana, M. Mendoza, S. Succi, and R. Tripiccione, Phys. Rev. E **95**, 053304 (2017).
- [23] A. Gabbana, M. Mendoza, S. Succi, and R. Tripiccione, Phys. Rev. E **96**, 023305 (2017).
- [24] R. C. V. Coelho, M. Mendoza, M. M. Doria, and H. J. Herrmann, arXiv:1706.00801 [cond-mat.soft].
- [25] I. Bouras, E. Molnár, H. Niemi, Z. Xu, A. El, O. Fochler, C. Greiner, and D. H. Rischke, Phys. Rev. Lett. **103**, 032301 (2009).
- [26] I. Bouras, E. Molnár, H. Niemi, Z. Xu, A. El, O. Fochler, C. Greiner, and D.H. Rischke, Nucl. Phys. A **830**, 741c–744c (2009).
- [27] I. Bouras, E. Molnár, H. Niemi, Z. Xu, A. El, O. Fochler, C. Greiner, and D. H. Rischke, Phys. Rev. C **82**, 024910 (2010).
- [28] G. S. Denicol, H. Niemi, E. Molnár, and D. H. Rischke, Phys. Rev. D **85**, 114047 (2012).
- [29] P. Romatschke, Phys. Rev. D **85**, 065012 (2012).
- [30] L. D. Landau and E. M. Lifshitz, *Fluid mechanics*, 2nd ed. (Pergamon Press, Oxford, UK, 1987).
- [31] C. Eckart, Phys. Rev. **58**, 919 (1940).
- [32] L. Rezzolla and O. Zanotti, *Relativistic hydrodynamics* (Oxford University Press, Oxford, UK, 2013).
- [33] W. A. Hiscock and L. Lindblom, Ann. Phys. **151**, 466–496 (1983).
- [34] A. El, Z. Xu, and C. Greiner, Phys. Rev. C **81**, 041901(R) (2010).
- [35] G. S. Denicol, T. Koide, and D. H. Rischke, Phys. Rev. Lett. **105**, 162501 (2010).

- [36] A. Jaiswal, Phys. Rev. C **88**, 021903(R) (2013)
- [37] C. Chattopadhyay, A. Jaiswal, S. Pal, and R. Ryblewski, Phys. Rev. C **91**, 024917 (2015).
- [38] A. Jaiswal, B. Friman, and K. Redlich, Phys. Lett. B **751**, 548–552 (2015).
- [39] J. A. Trangenstein, *Numerical solution of hyperbolic partial differential equations* (Cambridge University Press, New York, USA, 2007).
- [40] A. Jaiswal, Phys. Rev. C **87**, 051901(R) (2013).
- [41] L. Tinti, A. Jaiswal, and R. Ryblewski, Phys. Rev. D **95**, 054007 (2017).
- [42] E. F. Toro, *Riemann Solvers and Numerical Methods for Fluid Dynamics: A Practical Introduction*, 3rd ed. (Springer, Berlin, 2009).
- [43] G. S. Denicol and J. Noronha, arXiv:1608.07869 [nucl-th].
- [44] V. E. Ambruş and V. Sofonea, Phys. Rev. E **86**, 016708 (2012).